

“Analysis of Laser Metal Deposition Process against difference intensity models”

Major project-II

*Submitted to Delhi Technological University in partial fulfilment of the requirement for the
award of Degree of*

Master of Technology

In

Thermal Engineering

SUBMITTED BY-

Ashish Shukla

2K15/THE/03

UNDER SUPERVISION OF

DR. RAJ KUMAR SINGH

PROFESSOR



Department of Mechanical Engineering
Delhi Technological University
(Formerly DELHI COLLEGE OF ENGINEERING)

Bawana road, Delhi -110042

CERTIFICATE

DELHI TECHNOLOGICAL UNIVERSITY
(Formerly DELHI COLLEGE OF ENGINEERING)

This is to certify that report entitled “**Analysis of Laser Metal Deposition Process against difference intensity models**” by **Ashish Shukla** in the requirement of the partial fulfilment for the award of Degree of **Master of Technology (M.Tech)** in **Thermal Engineering** at **Delhi Technological University**. This work was completed under my supervision and guidance. He has completed his work with utmost sincerity and diligence. The work embodied in this project has not been submitted for the award of any other degree to the best of my knowledge.

Dr. Raj Kumar Singh

(Professor)

Delhi technological university

Delhi

DECLARATION

I declare that the work presented in this thesis titled “**Analysis of Laser Metal Deposition Process against difference intensity models**”, submitted to Department of Mechanical Engineering, is an authentic record of my own work carried out under the supervision of Prof. Dr.Raj Kumar Singh, Department of Mechanical Engineering, Delhi technological university, Delhi.

This report does not, to the best of my knowledge, contain part of my work which has been submitted for the award of any other degree either of this university or any other university without proper citation.

Date:

Place: DTU, Delhi

Signature of candidate

ACKNOWLEDGEMENT

It is a great pleasure to have the opportunity to extend my heartiest felt gratitude to everybody who helped me throughout the course of this major project.

It is distinct pleasure to express my deep sense of gratitude and indebtedness to my learned supervisors **Dr. Raj kumar singh** , Professor, in the Department of Mechanical Engineering, Delhi College of Engineering for their invaluable guidance, encouragement, and patient review. Their continuous inspiration only has enabled me to complete this major project.

I would also like to take this opportunity to present my sincere regards to my teachers for their kind support and encouragement.

I am thankful to my family members, friends and classmates for their unconditional support and motivation.

ASHISH SHUKLA

Abstract

Laser Direct Metal deposition (LDMD) is an additive manufacturing process, it is used to manufacture complex 3D objects directly from CAD files. Laser creates melt region on surface of substrate and powder material blown on to the laser-induced melt pool to form a layer. After a layer deposition, nozzle and laser assembly raised vertically upward by calculated small increment. Next layer is built on previous one, thus a 3D part is built layer by layer. Commercial available finite element tool ansys 14.0 is used to develop a numerically simulate heat transfer and coupled thermal phenomena to analyse the influence of various parameters (laser power, feed rate, laser velocity, etc.) on thermal history. Thermal cycles and its history experienced at different locations are studied and its influence is analysed. Influence of thermal loading on the model's distortion is analysed. As laser passed by the material the overall temp of the model is keep on increasing. Intensity distribution like Gaussian shoot the peak temperature of the subject higher than the distribution like frustum.

Table of Contents

ACKNOWLEDGEMENT	i
Abstract	v
List of figure	viii
Nomenclature	x
CHAPTER 1 Introduction.....	1
1.1 Laser metal deposition	1
1.2 Process.....	1
1.3 General characteristicsnof laser deposition.....	2
1.4 UsingnLMD to reducenmanufacturing costs	3
1.5 Advantages ofofna metallurgicalnbond.....	4
1.6 Technologicalnchallenges andneconomic benefits	5
1.7nAdvantages	6
1.8 Finitenelement method.....	7
1.9 Ansys.....	7
CHAPTER 2 LITERATURE REVIEW	8
2.1 Analysis of Heat Transfer	8
2.1 Analysis of coupled thermal (thermal plus structural).....	21
4.2 Conclusion from literature review.....	29
2.4 Problem Formulation and Gap Identification.....	31
CHAPTER 3 Methodology.....	32
3.1 Structure analysis	32
3.2 Thermal analysis	40
3.3 Combine (Multi-physics couple thermal analysis)	45
3.4 comparison between intensity distributions	49
Chapter 4 Results	54
Chapter 5 Conclusion and future scope	56

5.1 Conclusion.....	56
5.2 Future Scope.....	57
Reference:	58

List of figure

Figure 1: Schematic of LDMD process ^[1]	1
Figure 2: Same power and different time steps, (a) 2000W, 7.5s, (b) 2000W, 18.75s, (c) 2000W, 133.75s[2].....	9
Figure 3: Temperature time history of mid section[2].....	9
Figure 4: Influence of laser power on temperature gradient and cooling rate [2]	9
Figure 5: influence of scanning speed on temperature gradient and cooling rate [2].....	10
Figure 6: Variation of Temperature gradient with height and time[2]	11
Figure 7: Variation of temperature along first layer (a) and first eight layers (b) ^[3]	12
Figure 8 : Variation of temperature with different process parameters ^[3]	13
Figure 9: Thermal history of a point in the substrate (a) and in the deposit (b) ^[4]	14
Figure 10: Comparison between simulated and measured values at point A and B ^[5]	14
Figure 11: Sketch of the simplification of thermal history ^[7]	15
Figure 12: Actual and simulated melt pool profile ^[9]	17
Figure 13: Computed and measured width and height and computed thermal cycles ^[9]	18
Figure 14: Computed values of variation in cooling rate and comparison between estimated and measured cell spacing ^[9]	18
Figure 15: Comparison between estimated and measured micro-hardness in deposited layers ^[9]	19
Figure 16: Relation between temperature distribution and the trend of laser power and layer number (a) temperature distribution (b) trend of laser power changing ^[10]	19
Figure 17: Temperature field distribution with different radius ^[10]	20
Figure 18: Relationship between temperature distribution and radius ^[10]	21
Figure 19: Relation between building thickness and layer number, (a) with constant laser power, (b) with varied laser power ^[10]	21
Figure 20: Micrographs of deposits ^[11]	23
Figure 21: Comparison of melt pool boundaries obtained by the processing result of the edge detector with those obtained by the modelling,(a) original image acquired by high shutter speed camera, (b) processing result of edge detector, (c) numerical mode ^[11]	23
Figure 22: Distribution of residual stresses within subsequent layer, comparison between x-ray diffraction results and modelling results ^[11]	24
Figure 23: Comparison between experimental data and simulated values, (a) influence of laser power and mass feed rate on the stabilizing geometrical features of a DMD wall ^[12] ...	26

Figure 24: Comparison between experimental and simulated profiles (600 W, 0.006m/s), (a) thermocouple TC2, (b) TC3 (c) Temperature versus time simulated in the middle of the wall [12]	27
Figure 25: Comparison between (a) experimental (1000 Hz C-Mos fast camera), (b) simulated laser induced melt pool (600W, 0.006 m/s), between 2nd and 8 th manufactured layers [12].....	28
Figure 26: Residual stress on (a) top surface, (b) bottom surface of deposit along z direction [13]	28
Figure 27: Simulation and experimental results of deflection of substrate [13]	29
Figure 28 Model of bicycle.....	32
Figure 29 keypoints of model	33
Figure 30 Line model by keypoints	34
Figure 31 Meshed model of bicycle.....	35
Figure 32 Model with load and constraints.....	37
Figure 33 Solution of model	38
Figure 34 Deflection and real model	39
Figure 35 Stress analysis of model	40
Figure 36 Pre-processor	40
Figure 37 Selection of Element.....	41
Figure 38 Material properties.....	41
Figure 39 Rectangle model	42
Figure 40 Meshed model	42
Figure 41 Convection coefficient.....	43
Figure 42 Boundary conditions.....	43
Figure 43 Heat flux condition	44
Figure 44 Solution.....	44
Figure 45 Thermal results	45
Figure 46 model of thermo couple.....	46
Figure 47 Node of the model	47
Figure 48 Model of work ⁽³⁾	50
Figure 49 Nodal solution of temp.	53
Figure 50 Peak value temperatures corresponding to time stages ⁽³⁾	54
Figure 51 Compression between NODE A temp.....	54
Figure 52 Compression between NODE B temp.....	55

Nomenclature

V	Volume, m^3
ρ	Fluid density, kg/m^3
t	Time, s
u, v	Velocity magnitude in directions x,y, m/s
P	Pressure, Pa
λ	Viscosity coefficient
μ	Dynamic viscosity, Pa/s
e	Internal energy per unit mass, J/kg
k	Turbulent kinetic energy, m^2/s^2
ε	Turbulent dissipation rate, m^2/s^3
μ_t	Turbulence viscosity, Pa-s

CHAPTER 1 Introduction

1.1 Laser metal deposition

The principle of laser deposition consists of fusing a metal filler material and a very thin layer of the surface of the substrate to ensure a metallurgical bond. The laser beam is then a vector of a precise and localized heat input. Material is mainly brought in the form of powder, which offers the advantage of depositing a very wide choice of metal materials. The powder is injected laterally or coaxially into the laser beam. If the first technique shows great simplicity, it should be noted that a difficult control of the injector position in relation to the direction of travel is necessary to do complex shapes. This factor explains the major use of coaxial devices that thus allow multidirectional cladding. In addition, since the irradiation of the filling material is slower and more regular than during lateral injection, the evenness of the deposition and the yield of deposition of the whole are higher.⁽¹⁾

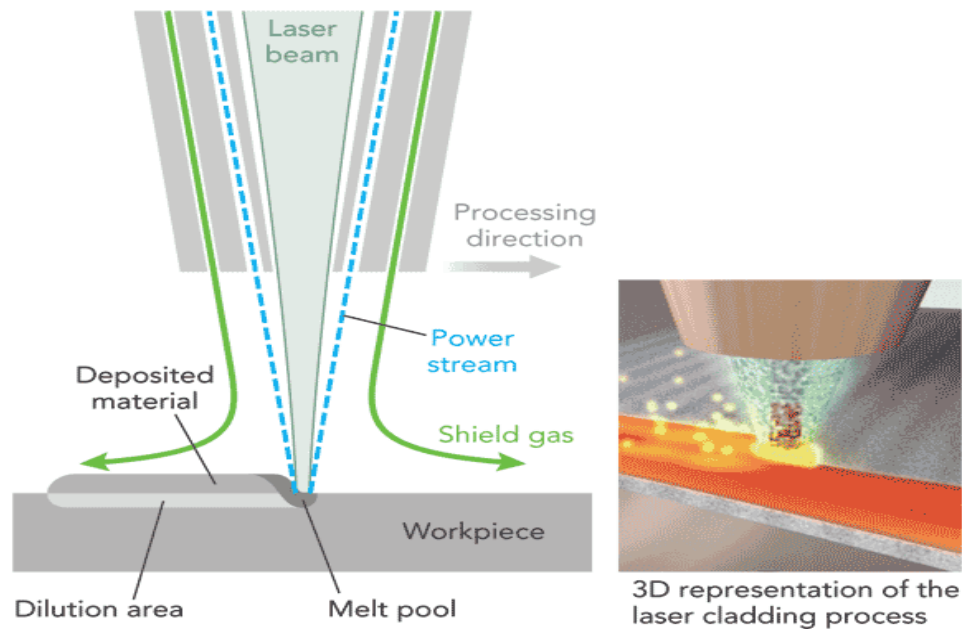


Figure 1: Schematic of LDMD process^[1]

1.2 Process

The powder used in laser cladding is normally of a metallic nature, and is injected into the system by either coaxial or lateral nozzles. The interaction of the metallic powder stream and the laser causes melting to occur, and is known as the melt pool. This is deposited onto

a substrate; moving the substrate allows the melt pool to solidify and thus produces a track of solid metal. This is the most common technique, however some processes involve moving the laser/nozzle assembly over a stationary substrate to produce solidified tracks. The motion of the substrate is guided by a CAD system which interpolates solid objects into a set of tracks, thus producing the desired part at the end of the trajectory.

A great deal of research is now being concentrated on developing automatic laser cladding machines. Many of the process parameters must be manually set, such as laser power, laser focal point, substrate velocity, powder injection rate, etc., and thus require the attention of a specialized technician to ensure proper results. However, many groups are focusing their attention on developing sensors to measure the process online. Such sensors monitor the clad's geometry (height and width of deposited track), metallurgical properties (such as the rate of solidification, and hence the final microstructure), and temperature information of both the immediate melt pool and its surrounding areas. With such sensors, control strategies are being designed such that constant observation from a technician is no longer required to produce a final product. Further research has been directed to forward processing where system parameters are developed around specific metallurgical properties for user defined applications (such as microstructure, internal stresses, dilution zone gradients, and clad contact angle).⁽¹⁸⁾

1.3 General characteristics of laser deposition

The intrinsic characteristics of laser cladding ensure:

- *The metallurgical quality of the deposits.* The bond of metallurgical type guarantees very low risks of delamination, and the fusion of the filler material makes it possible to obtain a dense deposition. The characteristics of the deposition depend on the chemical composition of the filler material used. A wide variety of materials may be deposited, like iron bases (carbon steel, stainless steel, tool steel, etc.), cobalt bases (Stellite), nickel bases (Inconel, Hastelloy, etc.), titanium bases, and aluminum alloys, among others. The speed of the thermal cycle makes it possible to obtain very fine microstructures and higher hardnesses than traditional welding and cladding techniques. In general, these fine structures increase resistance to corrosion. In the case of metal matrix compounds (MMCs),

laser cladding avoids the fusing of hard compounds (generally carbides), which remain present in a metal matrix. It should, however, be noted that this technique of fusion cladding can lead to defects related to stresses, metallurgical incompatibility of materials, or even the compounds formed in the bonding area between deposition and substrate⁽¹⁾.

- *A very low dilution.* In laser treatment, dilution (namely the participation of the substrate in the deposition) is controllable and low (less than 5% in the case of steel), which allows good conservation of properties of the deposited material. Among other things, this particularity limits the number of layers required for obtaining a particular chemical composition on the surface⁽¹⁾.
- *The respect of the geometry.* The speed of the thermal cycle and the low heated volume have the effect of limiting the trauma suffered by the part. The heat-affected zone (HAZ) is reduced and the deformations are then lower than with other processes, while the location of the thermal impact also allows work in critical areas in term of thin adjacent walls, edges, etc. The automated process allows a high degree of accuracy of trajectory and low machining times when these are needed.⁽¹⁾

1.4 Using LMD to reduce manufacturing costs

Using LMD workpiece properties can be targeted for improvement by systematically refining or combining materials. For example you can give a softer metal a hard, high-quality surface; combine a thermally insulating material with a conductive layer; or coat metal with materials that resist high temperatures, salt water, or chemicals. Laser deposition will not only lengthen the life of your components, it will also significantly reduce the overall manufacturing costs⁽¹⁷⁾.

How can critical parts operating in tough environments be made to last longer? How can these valuable components be repaired so that their lifetime cost is lower? LMD might be the solution. It has been around since the 1970s when teams of scientists from places like Avco Everett Research Lab were performing every application that they could think of with their high-powered gas lasers. However, LMD hasn't become a mainstream

application like laser cutting. The reasons might be that the capital cost has been too high to justify the process as compared to other heat sources, or the price for a new component was too low to justify a repair. Maybe the LMD process was not considered robust or repeatable enough to be used in more than a few select applications where there was simply no other practical solution. Regardless, it is a viable process that has been under-utilized until recently. The advent of higher-powered lasers, with beams that can be delivered through fibers and integrated into robust machine tools, decreased capital investment and operating costs of the laser device. This, in combination with the significantly increased cost of metals and the use of higher-performance materials, has caused many to rethink the use of the LMD process while producing new components or repairing used ones ⁽¹⁷⁾

1.5 Advantages of a metallurgical bond

Extreme processes and competitive industries now require their components to have extremely long uptimes and high reliability, and for this they require processes that can extend the life of the parts. LMD produces a metallurgical bond that permanently attaches the deposited metal onto the base material, creating the best possible adhesion. The process itself is relatively simple: a laser beam produces a weld pool on the surface of a component. Powder jets blow a metallurgical powder into the weld pool coaxially to the working beam; the powder melts and is metallurgically bonded onto the base material. This enables new layers of metal with defined properties to be applied, even against the force of gravity (see FIGURE 2). Depending on the application, individual materials or powder mixtures consisting of different materials can be used, allowing the properties of the new layer to be very precisely defined. Iron, cobalt, titanium, and nickel alloys, as well as materials containing carbide, are all applicable. It is possible to choose a powder composition and the laser power in such a way that the carbides have a homogeneous distribution in the layer. For example, this enables tungsten or titanium carbides to be embedded into the deposited metallic matrix to increase the wear resistance of the component surface. ⁽¹⁷⁾

Other processes are also used in the deposition of powder (and wire), but there are significant limitations to consider. Some create a mechanical bond that does not hold as well as a metallurgical bond so that the coating fails sooner, requiring replacement or repair. Others require significantly more heat to melt both the powder and base material, which distorts the component to a higher degree, requiring a secondary operation to put it back into tolerance. The excess heat also causes heavy dilution of the base material into the

coating, requiring two or three extra coating passes to achieve the chemical characteristics of the deposited material. This consumes significantly more powder, which is usually quite expensive, and of course requires more heat, which further distorts the part requiring even more post-process machining. The LMD process creates so little dilution that the coating is "at chemistry" within a few thousandths (~50-70 microns) and a coating depth of 0.060 inch (1.5 mm) is often all that's needed since the entire depth will be pure material.⁽¹⁷⁾

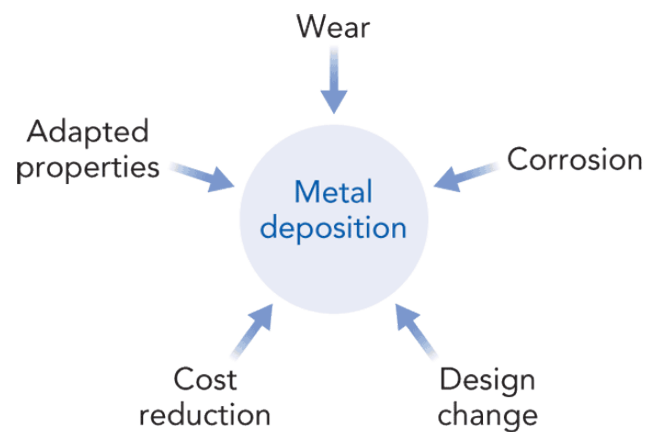


fig1. The LMD process enables new layers of metal with defined properties to be applied, even against the force of gravity.⁽¹⁷⁾

1.6 Technological challenges and economic benefits

Despite its huge potential, laser deposition welding long remained a process confined to the laboratory. The main challenge lay in adequate process control – to achieve a homogeneous layer with the specified properties, the laser power, powder composition and the supply, frequently of multiple materials, must be precisely coordinated and controlled. However, manufacturers such as TRUMPF now offer complete technology packages for laser material deposition applications that guarantee proper control of these aspects.⁽¹⁷⁾

They normally consist of three functional units – the powder feed, the processing optics with powder jet and the powder transfer line (which connects the feeder), and the optical system. For TRUMPF systems, the powder feed is normally a mobile unit with up to four

independently programmable powder containers. The feeder combines the powder/gas mixture from the containers into a precisely adjusted powder mass flow. Sensors continuously monitor the composition of the flow, ensuring that there are no fluctuations in the metallurgical composition of the layer.

The economic benefits of this technology lie in the ability to add value to the component by depositing a layer or layers of material to significantly increase the operating life of expensive components that need to function reliably for long periods of time in expensive processes. The layer's properties allow operation in increased temperature or better corrosion and wear resistance.⁽¹⁷⁾

The marine engine industry also wants to repair used components, although the value of the material is not nearly as high as blisks (portmanteau of bladed disk). Instead, they are interested in ways to more easily and economically repair large quantities in a highly automated way. On the pistons in four-stroke auxiliary diesel engines, there is increased load on the first piston ring groove. This is more directly exposed to corrosion from the combustion gases and wear from hard particles in the fuel than the subsequent piston ring grooves. As a result, substantial wear can often be seen here, although the piston itself only demonstrates minimal wear, such as burnout on the piston crown. However, the damage from the ring groove wear is so significant that the entire piston has to be replaced or repaired. Until recently, there were no appropriate repair processes that enabled the original geometry of the groove to be restored. The requirements are good accessibility to the tight geometries, high precision and reproducibility, no damage to the basic material, no thermal distortion, a high level of automation, reduction of post-processing due to precise deposition location and thickness, and improvement of wear properties by selection of appropriate coating materials. Conventional deposition welding processes cannot achieve all of these requirements, particularly accessibility, reproducibility, and low thermal loads⁽¹⁷⁾

1.7 Advantages

- Best technique for coating any shape increase life-time of wearing parts.
- Particular dispositions for repairing parts (ideal if the mould of the part no longer exist or too long time needed for a new fabrication).
- Most suited technique for graded material application.
- Well adapted for near-net-shape manufacturing.

- Low dilution between track and substrate (unlike other welding processes and strong metallurgical bond).
- Low deformation of the substrate and small heat affected zone (HAZ).
- High cooling rate fine microstructure.
- A lot of material flexibility (metal, ceramic, even polymer).
- Built part is free of crack and porosity.
- Compact technology.⁽¹⁷⁾

1.8 Finite element method

The finite element method (FEM) is a numerical method for solving problems of engineering and mathematical physics. It is also referred to as finite element analysis (FEA). Typical problem areas of interest include structural analysis, heat transfer, fluid flow, mass transport, and electromagnetic potential. The analytical solution these problems generally require the solution to boundary value problems for partial differential equations. The finite element method formulation of the problem results in a system of algebraic equations. The method yields approximate values of the unknowns at discrete number of points over the domain. To solve the problem, it subdivides a large problem into smaller, simpler parts that are called finite elements. The simple equations that model these finite elements are then assembled into a larger system of equations that models the entire problem. FEM then uses variation methods from the calculus of variations to approximate a solution by minimizing an associated error function.⁽¹⁸⁾

1.9 Ansys

ANSYS Mechanical is a finite element analysis tool for structural analysis, including linear, nonlinear and dynamic studies. This computer simulation product provides finite elements to model behaviour, and supports material models and equation solvers for a wide range of mechanical design problems. ANSYS Mechanical also includes thermal analysis and coupled-physics capabilities involving acoustics, piezoelectric, thermal–structural and thermo-electric analysis.⁽¹⁸⁾

CHAPTER 2 LITERATURE REVIEW

2.1 Analysis of Heat Transfer

Direct Metal Deposition is a process of shock cooling and heating and the distribution and variation of temperature field has important influence on microstructure, quality, formation of cracks etc, Song et al^[2] studied the temperature-time history curves, temperature field distribution, cooling rate and the temperature gradient of the laser cladding forming process. Influences of laser power and scanning speed on the temperature gradient and cooling rate of the cladding layers have been studied, which provided explanation of microstructure forming mechanism, cracking sensitivity and parameter selection. At the same time, LCF experiments have been conducted with parameters obtained from the simulation, microstructure of the cladding layers have been analysed.

Three-dimensional transient temperature fields were studied with finite element methods, the temperature gradient and cooling rate of Laser Cladding Forming were extremely high, reached 105-106 °C /m and 103-104 °C /s, respectively. Laser power and scanning speed have an significant influence on the size of the melting pool, the cooling rate of the solid-liquid interface and the temperature gradient of the cladding layers, therefore laser power should be adjusted with the proceeding of the processing and the scanning speed should not be too large to prevent cracks.

At the bottom of the melting pool, the temperature gradient G is very large and the cooling rate is very small, the temperature gradient perpendicular to axis Z is predominated. From the bottom to the top of the melting pool, the temperature gradient along axis X increases gradually and the component of axis Z decreases gradually. At the top of the top surface, the temperature gradient along the horizontal exceeds that of the perpendicular direction.

- 316L stainless steel powder as cladding material (melting point 1400 C).
- Common carbon steel 45 as substrate.
- Specific heat and thermal conductivity of 316L stainless steel is time dependent
- Figure 2 shows Laser power 800-3000W, scanning speed 50-240mm/min and spot size 4 x 4 mm² (Laser power, scanning speed and spot size decides temperature field, temperature gradient and cooling rate of melt pool which in turn decides morphology and crack susceptibility).

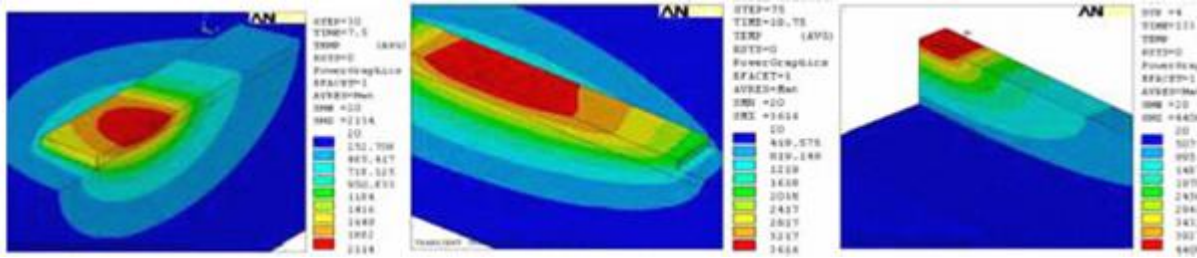


Figure 2: Same power and different time steps, (a) 2000W, 7.5s, (b) 2000W, 18.75s, (c) 2000W, 133.75s[2]

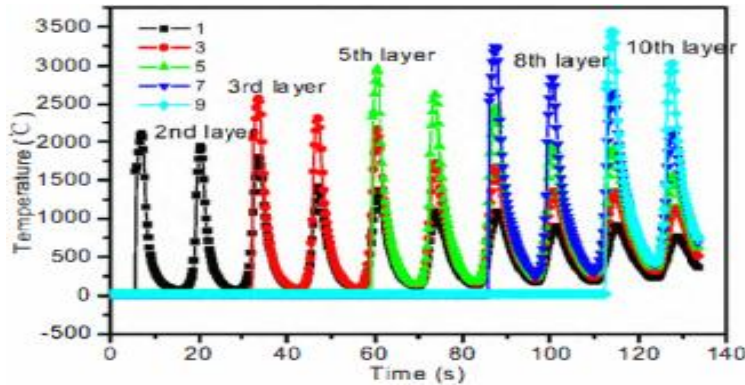


Figure 3: Temperature time history of mid section[2]

- Quick heating leads to high temperature gradient and cooling rate of melt pool.
- High laser power, temperature difference between cladding layer and substrate was smaller.

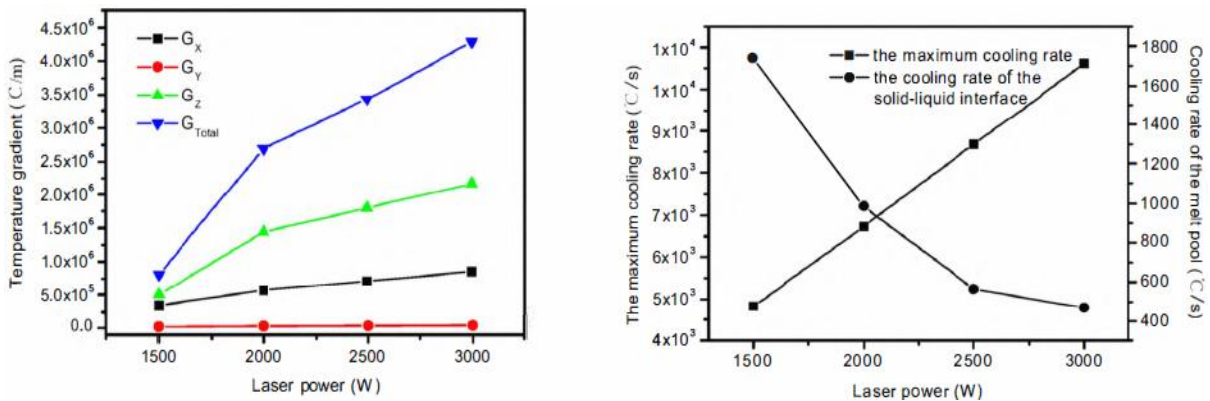


Figure 4: Influence of laser power on temperature gradient and cooling rate [2]

- In Figure 4 first is for melt pool and second is for solid liquid interface. Cooling rate along solid liquid interface has important influence to microstructure and cracking tendency of cladding layer. Temperature gradient is constant for y axis with increase of laser power, for x axis temperature gradient is increasing with the rate of 333.3°C/m for increase of one watt power after 1500W, for z axis 1000°C/m for increase of one watt power after 1500W, for overall 2666.67°C/m for increase of one watt power after 1500W (approx.). For cooling of melt pool the maximum cooling rate

is $3.43^{\circ}\text{C}/\text{sec}$ for increase of one watt power after 1500W and the cooling rate is $1.6^{\circ}\text{C}/\text{sec}$ for 1500 to 2000W power, $1^{\circ}\text{C}/\text{sec}$ for 2000 to 2500W power, $0.2^{\circ}\text{C}/\text{sec}$ for 2500 to 3000W. High laser power temp difference between cladding layer and substrate was smaller, therefore lower cooling rate.

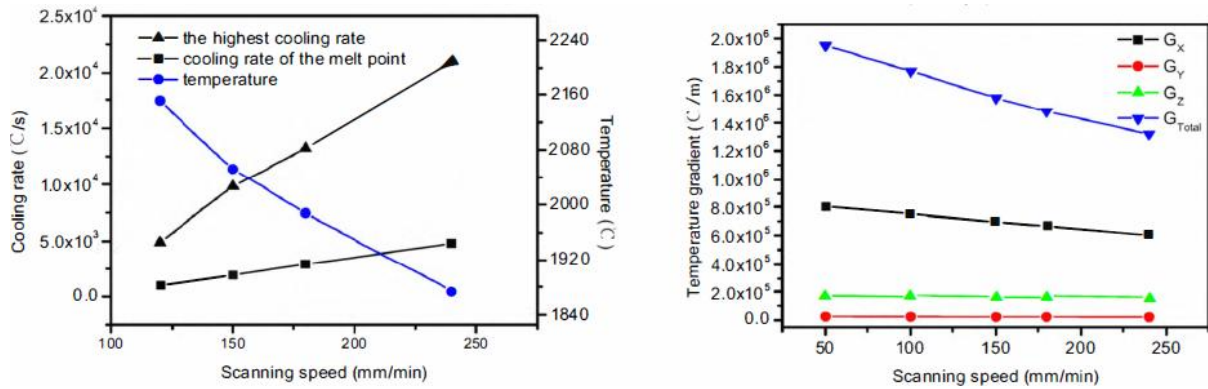


Figure 5: influence of scanning speed on temperature gradient and cooling rate [2]

- As scanning speed increases, highest temperature and gradient decreases, while cooling also decreases. The cooling rate of cladding layer is $30^{\circ}\text{C}/\text{sec}$ for increase of 1mm/min speed after 100mm/min speed. Whereas the maximum cooling rate $120^{\circ}\text{C}/\text{sec}$ for 1mm/min speed after 100mm/min speed. The temperature decreases by 260°C for initial 125mm/min to 150mm/min, further decreases by 350°C for 150mm/min to 250mm/min. The temperature gradient is constant with scanning speed of 50mm/min to 250mm/min for y axis and z axis, for x axis decreases by $500^{\circ}\text{C}/\text{m}$ for scanning speed 50mm/min to 250mm/min, overall temperature gradient is $2500^{\circ}\text{C}/\text{m}$ for scanning speed 50mm/min to 250mm/min. Because too higher scanning speed will result in a poor bonding strength and higher sensitivity of cracking, appropriate scanning speed should be used in order to obtain better forming qualities (Figure 5).
- At bottom of cladding layer, temp gradient along z was biggest and decreases as goes to upper layers. Figure 6
- At upper layers x gradient is more than z.

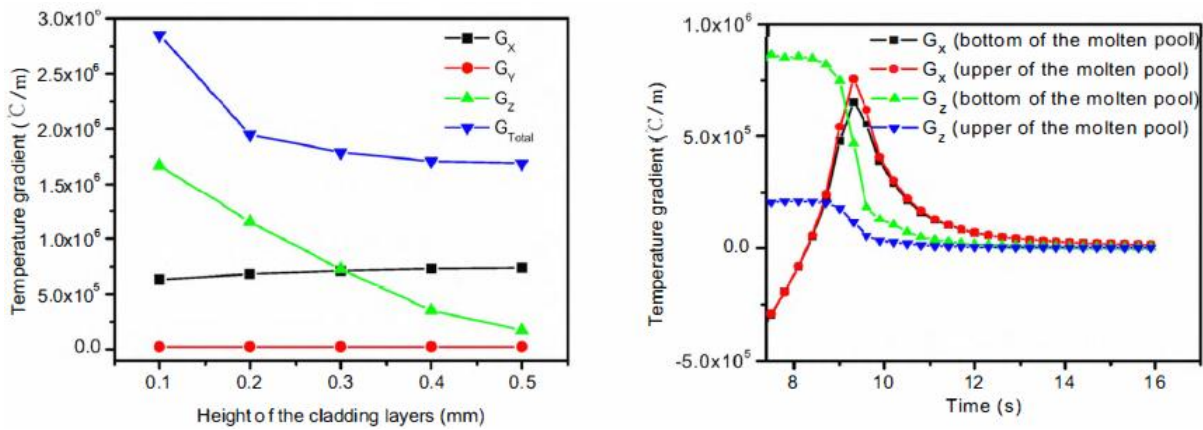


Figure 6: Variation of Temperature gradient with height and time[2]

- heat flow via the substrate is no longer predominating, the heat of the cladding layers radiates through the environment, which can be seen from Figure 6 that at the bottom of the melting pool, temperature gradient along axis Z is predominating while at the top of the melting pool, the gradient along axis X is the maximum.

Peak temperature and thermal cycle experienced by each layer influence the final mechanical properties and dimensional accuracy of the part. An understanding and quantitative knowledge of the peak temperature, melt pool dimensions, and thermal cycles experienced in the deposited layers are essential for a priori selection of the process parameters in LENS technique. Neela et al^[3] numerically simulate heat transfer phenomenon in LENS process considering deposition of SS316 powders on a substrate of the same material. The computed temperature profiles are first validated with experimental results reported in the literature. The influence of process parameters on peak temperature, thermal cycle and melt pool dimensions are studied subsequently. The temperature distributions are first computed corresponding to the deposition of a multi-layered thin wall structure (length/width/height ~12:2:6.25mm) into a substrate (length/width/height ~12:6:2 mm) using a laser power and scanning velocity of 275 W and 7.62 mm/s, respectively. Average powder mass flow rate of 3 g/min is considered a layer increment of 250 μm is followed. Figure 7 depicts the computed results of the temperature profile against the corresponding measured results at location 1.6 mm away from the centre of the laser beam along the topmost layer. The horizontal line in Figure 7 indicates the liquidus (melting) temperature of SS316 (1,733 K) and meets both the computed and the corresponding measured temperature profiles at their point of intersection.

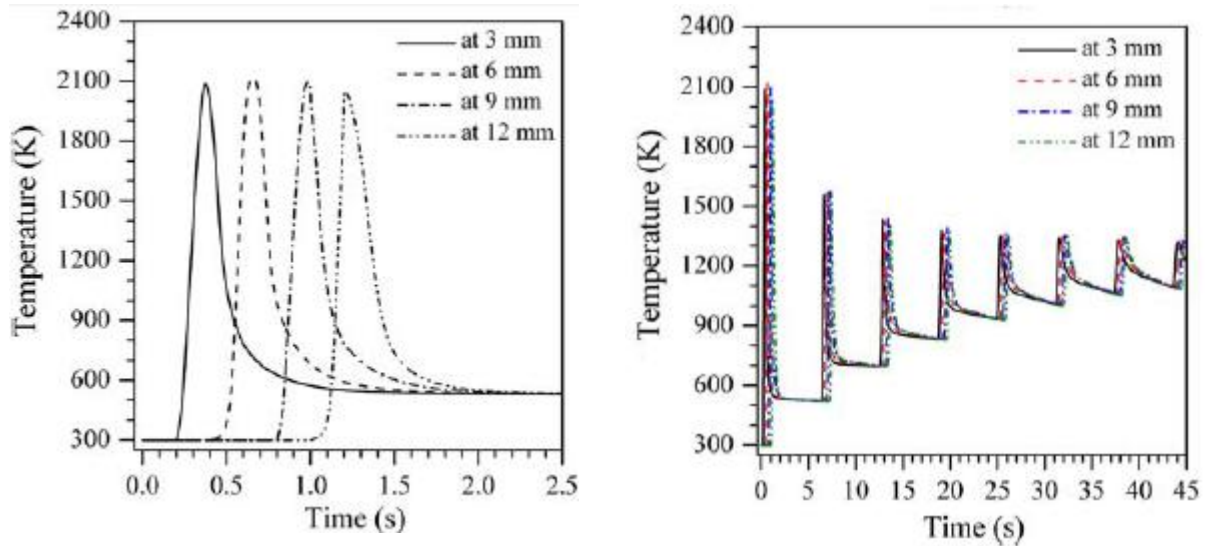


Figure 7: Variation of temperature along first layer (a) and first eight layers (b)^[3]

Figure 7 (a) shows the computed thermal cycles experienced at different linear locations (3, 6, 9, and 12 mm) on the first layer corresponding to a laser power of 400 W, focused beam radius of 1 mm, scanning velocity of 10 mm/s, and a powder mass flow rate of 4 g/min with 60% catchment efficiency. Figure 7 (b) depicts similar computed thermal cycles on the same locations, however, during the building of the first to eighth layers corresponding to the same set of process variables. It is observed in Figure 7 (a) that as the laser beam reaches or is near a particular location, peak temperature shoots to nearly 2,100 K followed by a rapid cooling as the beam moves away. Figure 7 (b) indicates that the peak temperature along the first layer reduces continually as the build height increases and the laser beam also moves up. However, the resident temperature of any layer increases continually. The computed temperature history in Figure 7 (b) conforms to a duration of 1.2 s for the deposition of each layer and an idle time of 5 s between two successive layers, leading to a total time of 44.6 s for completely depositing eight layers.

Figure 8 (a), (b) depicts the influence of laser power (P), scanning velocity (v), powder mass flow rate (f), and idle time (t -idle) on the computed values of peak temperature and overall thermal cycle at the initial location on the first layer during the deposition of subsequent layers atop it. Figure 8 (a) shows that both the peak temperature and the resident temperature rise with increasing laser power. This is attributed to the increase in net heat input corresponding to greater laser power. Figure 8 (b) shows that the resident temperature reduces with the increase in the idle time. Jia Yang et al^[4] describe the thermal dynamics behaviour in direct laser fabrication (DLF), a model is proposed to be built/ developed based

on global model and sub-model pattern. The global model exhibits the heat conduction characteristics of parts in the whole thermal history according to scanning path planning. Contact pairs and gap elements, which consider the effect of the temperature and porosity dependent thermal conduction, are designed in the model to explain powder-to-solid intrinsic transition. The influence of non-linear behaviour of thermal properties in pure nickel on the temperature distribution is estimated as well. Adopting the thermal physical parameters with solid-liquid phase change will make the melted pool temperature higher than that where the solid-liquid phase change parameters are not considered.

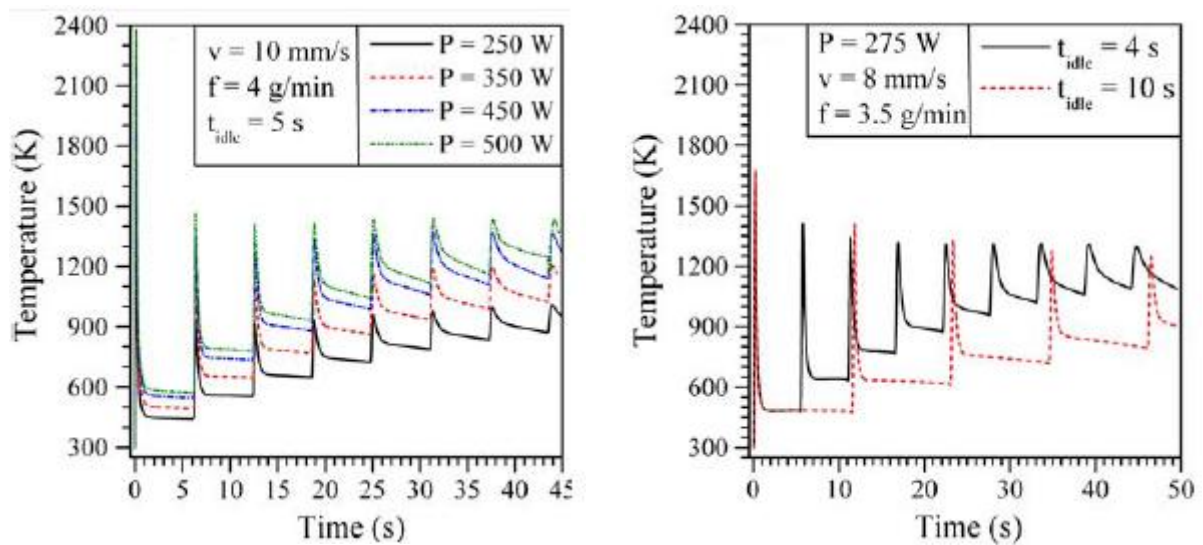


Figure 8 : Variation of temperature with different process parameters^[3]

It was observed that in the deposition (some point was taken) due to solid-liquid phase change parameters, the melting point temperature attains higher temperature at time 0.72 second. Without influence of solid-liquid phase change parameters the melting point temperature attained at time 0.72 second is lesser. Temperatures on the other locations are higher than the first case however.

It can be seen that studies of the above mentioned work focus on the thin wall with no more than ten deposited layers. Yongjie Zhang et al^[5] built 200 layers of SS410 by LDMD process, (substrate material was set to SS316). Influence of thermal history on microstructure and properties of a multilayer stainless steel (SS410) thin wall built by laser direct metal deposition (LDMD) process was investigated experimentally and numerically by 2 thermocouples. Simulated and measured thermal history indicated that the absorption and loss of heat tended to be close to equilibrium when the deposited material reached a certain

height during the LDMD process. Different microstructure regions were formed due to the different thermal history the material experienced. The hardness distribution along the height centreline of the thin wall was measured. The results indicated that thermal history had an important effect on the

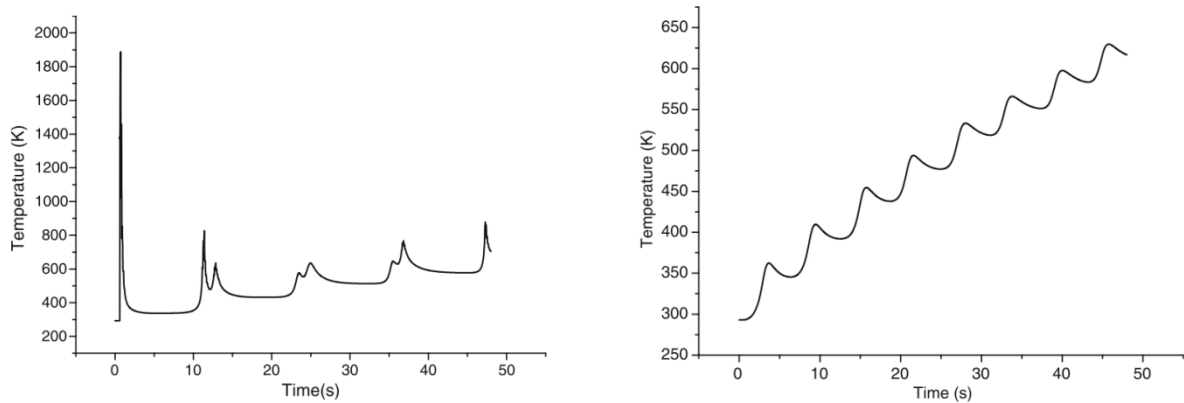


Figure 9: Thermal history of a point in the substrate (a) and in the deposit (b)^[4]

Experimental procedure: (Figure 10)

- SS410 deposition on SS316 as substrate (same thermophysical prop but different microstructure)
- Cross sectioned by wire electrode
- Optical microscopy (OM) and scanning electron microscopy (SEM) coupled with an energy-dispersive spectrometer (EDS) were used to investigate the microstructure. X-ray diffraction (XRD) was used for phase identification.

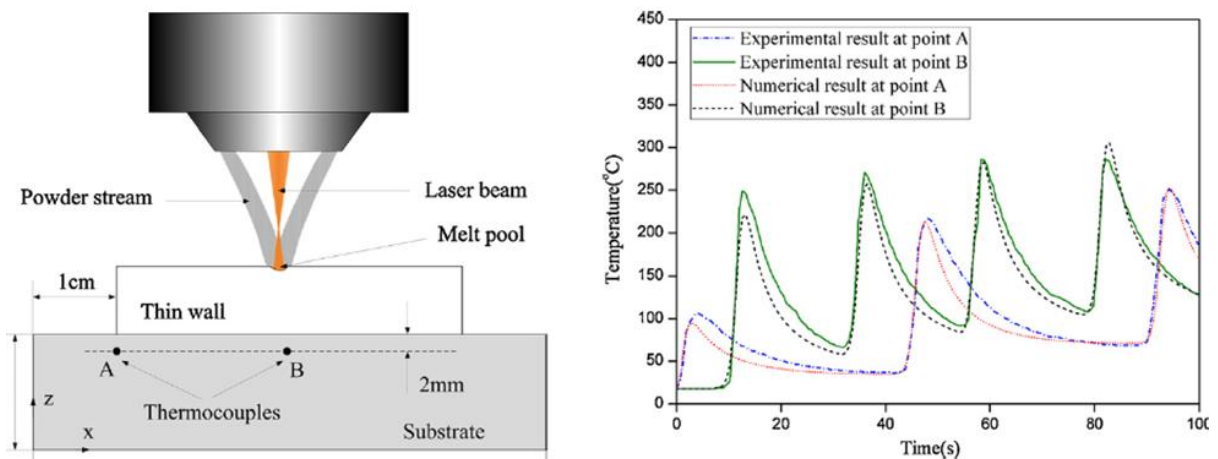


Figure 10: Comparison between simulated and measured values at point A and B^[5]

The temperature reached a peak every time the laser beam passed over the measuring point, and then decreased to a resident temperature. Thermal cycle period at point A was the double of that at point B. However, thermal history at the two points had the same changing trend.

Wang et al. (2008)^[6] found the similar phenomena and they concluded that the decreasing laser power was required to keep a constant pool size as more layers were deposited.

To make the property analysis from thermal history easier, Zhang Yongjie et al ^[7] define a critical temperature specific to thermal history and the distribution of it in the part was also discussed. The simulation results indicated that the critical temperature can make the property analysis from thermal history easier. Thermal history of all the deposited materials was similar. It was also concluded that process parameters needed to be time-varying according to the real-time temperature field during the process.

Characteristics of thermal history of points other than mid points are generally not covered and only few layers considered in earlier papers in this paper other points are also being covered and analysis has been done on many layers.

- Thermal history of deposited material at location A, B and C of layers 1, 5 and 10
- Fluctuations tend to dampen as more layers are deposited.
- Peak temperature falls continually
- Resident temperature of cycle increases

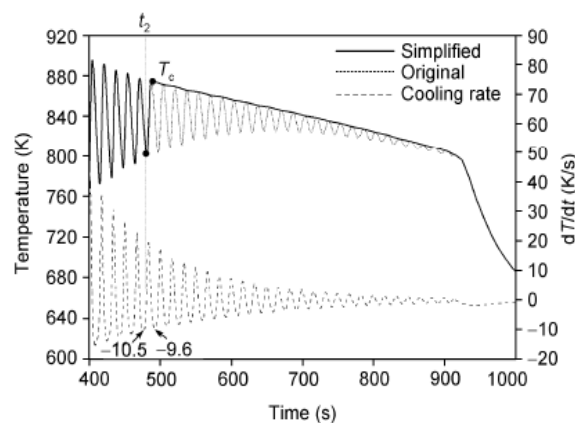


Figure 11: Sketch of the simplification of thermal history^[7]

There is also a local minimum of 10k/s *at the midpoint of each layer. This is because a* short time interval of laser irradiations allows less thermal energy to be dissipated. As more layers are deposited, the energy accumulates and the whole temperature of the part increases.

- 10K/s is chosen as critical cooling rate
- Region (t2 till end) can be treated as 1 cycle, peak temp Tc then cools down to room temp.

All the thermal histories of the deposited materials of the part are similar. It can be considered as a sequence of thermal cycles. During the initial stage, the deposited materials experience a significant rapid quenching effect and can attain a very high cooling rate of 103 K/s. Then the peak temperature of thermal cycle decreases and the resident temperature increases continually as the subsequent layer atop it increases. When the deposited materials above reach a certain thickness, the rapid quenching effect decreases and even disappears.

The thermal history of the deposited materials which is dependent on the process parameters has significant influences on the geometric precision and mechanical properties of the final part. Thus better properties can be obtained by maintaining a predetermined steady melt pool temperature field, which requires time-varying process parameters according to the real-time temperature feedback. Atul et al^[8] simulated the temperature distribution and single track geometry in Laser Rapid Manufacturing using two dimensional model, and calculated excessive enthalpy above melting point, laser beam size and profile, scan speed, powder feed rate and powder stream diameter with flow distribution is taken from the user. Capability of developed algorithm was demonstrated by depositing single track on SS316L work piece using Inconel 625 at simulated process parameters. Manavatkar et al^[9] Computed values of cooling rate during solidification used to estimate variation in cell spacing of solidified structure. Hall-Petch like relation using cell size as structural parameter is used to estimate hardness distribution. Estimated values of layer-wise cell spacing and hardness remain under predicted and over predicted. Dendrite arm spacing λ used to estimate cooling rate Cr by empirical relation

$$\lambda_2 = A(C_R)^{-n}$$

Where, 'A' and 'n' are material constant.

Grain size is used to measured harness (Hall-Petch)

$$\sigma_y = \sigma_0 + k_y(d_g)^{-0.5}$$

σ_y and d_g refer to yield strength and grain size, σ_0 and K_y refers to lattice resistance and a factor. Attempts are made to numerically predict the influence of process parameters on thermal cycle, residual stress, microstructure, micro hardness in deposits of SS304, SS316 and various tool steels.

Hall-petch equation: the equation indicates that strength of metal is equal to frictional stress plus a factor K times the inverse of square root of grain size D . reducing grain size will cause the material to become stronger also increase the toughness.

Cell spacing (or grain size) taken as $3\mu\text{m}$, 3D FE model will predict peak temp, melt pool dimension, cooling rate. Cooling rates will be used to estimate layer-wise cell spacing. Cell spacing will be used to estimate micro hardness by Hall pech relation. Results are validated with actual multilayer deposit of SS316.

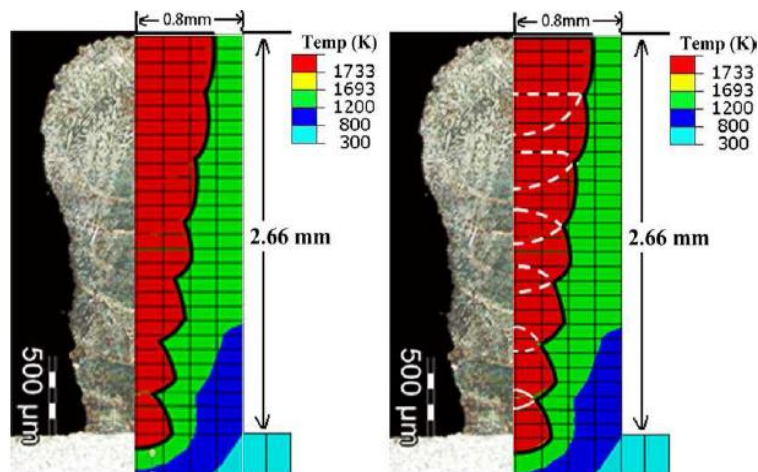


Figure 12: Actual and simulated melt pool profile^[9]

- First half of Figure 12 compares actual deposited profile of 7 layers, thick black line is 1733K isotherm.
- Second half of Figure 12 shows simulated melt pool profile.
- White lines also correspond to 1733K isotherm, in dashed since they are inside the pool.
- Reasonable agreement between computed and measured melt pool width and total build height.
- Slight under prediction due to heat transfer to un-melted powder, as broader the 1733K isotherm broader will be the layer thickness.

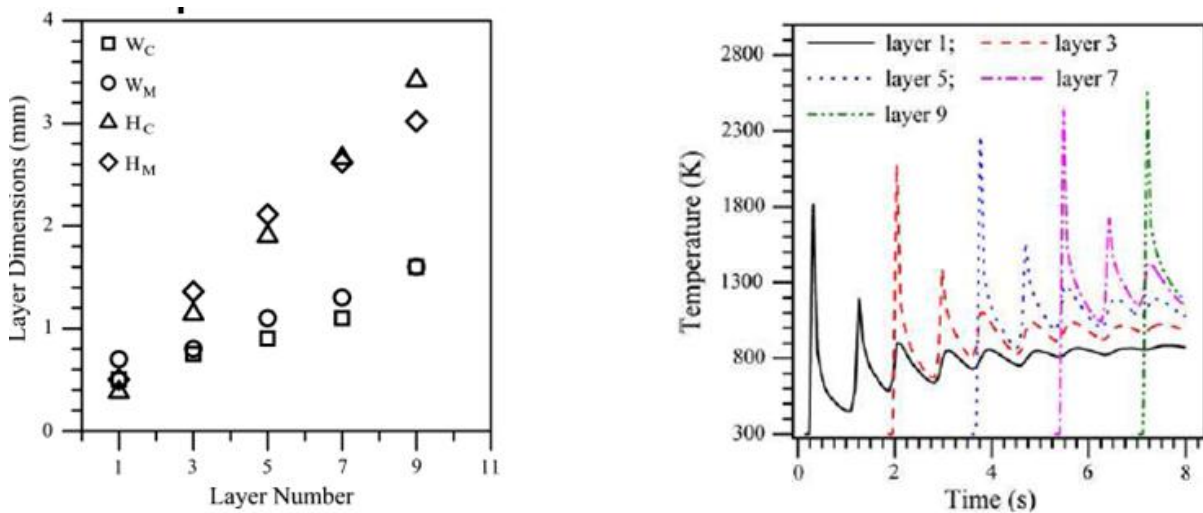


Figure 13: Computed and measured width and height and computed thermal cycles ¹⁹¹

- Cooling rates reduces with layer deposition.
- High cooling rate in bottom layer due to rapid heat loss through original substrate.
- Cell spacing increase with built height due to decrease in cooling rate.
- Underestimation of cell spacing is due to over prediction of cooling rates.
- Solidification is columnar in all layers.
- Cell orientation follows direction of maximum thermal gradient.
- Hardness decreases with increase in built height.
- Due to reduction in cooling rate and resulting increase in cell spacing.

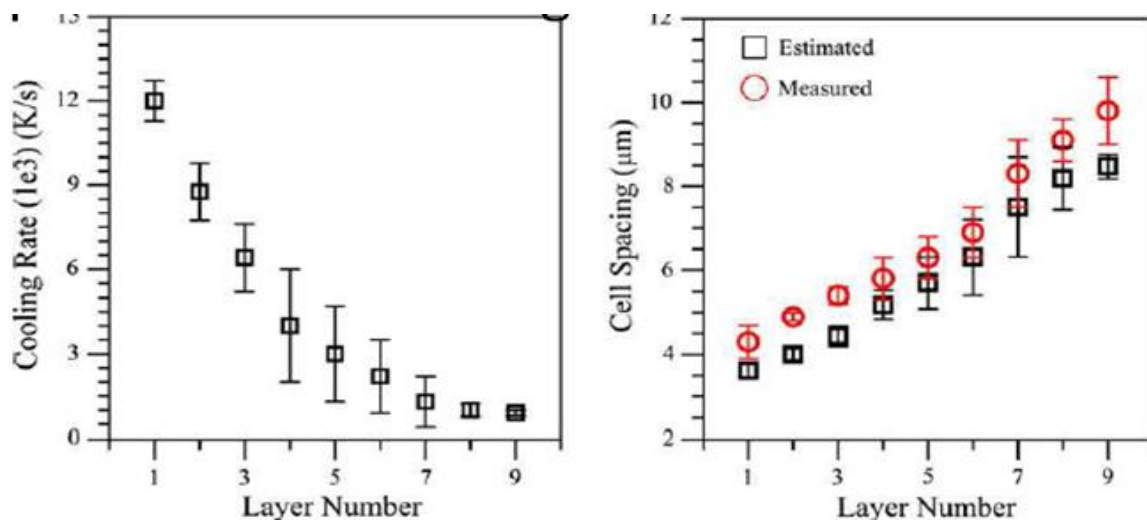


Figure 14: Computed values of variation in cooling rate and comparison between estimated and measured cell spacing ¹⁹¹

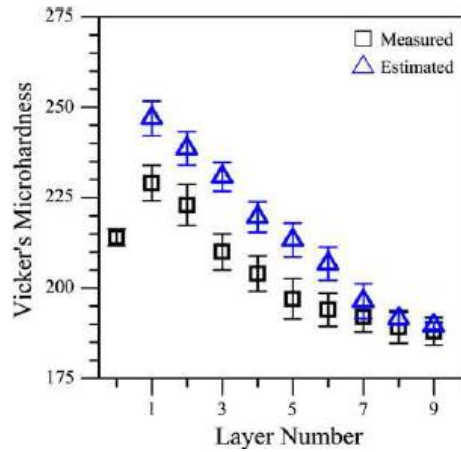


Figure 15: Comparison between estimated and measured micro-hardness in deposited layers ^[9]

Gangxian Zhu et al^[10], discussed the effect of curvature change and accumulation of layers on the temperature field distribution, and was investigated by thin walled rings with different curvatures. It was observed from the numerical results that the temperature of thin wall increases with layer number and its curvature. The rules for changing laser power with layer number and curvature in the processing of thin walled blade can be obtained by simulation when keeping the molten pool temperature stable.

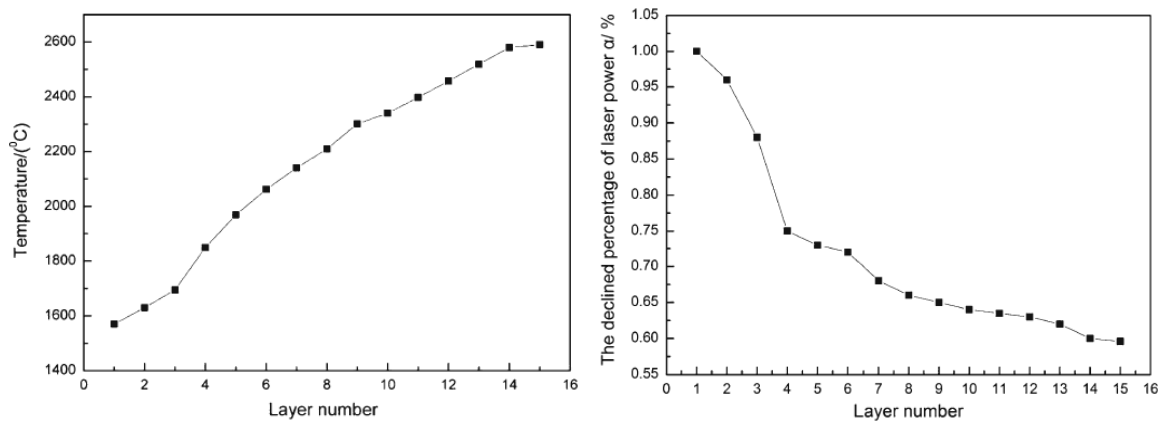


Figure 16: Relation between temperature distribution and the trend of laser power and layer number (a) temperature distribution (b) trend of laser power changing ^[10]

The model was used to simulate the entire 15-layer LDMD process. Temperature distributions with layer number were shown in Figure 16 (a) above under constant laser power condition. Based on the 1,570°C produced by temperature field computation of the first deposited layer, the trend of laser power changing could be obtained with layer by layer by keeping a constant molten pool temperature, as shown in Figure 16 (b).

It is observed from Figure 16 (a) that the calculated temperature increases with the layer number. Because the substrate is cold during deposition of the first few layers, and as more layers are deposited, they act as a barrier to heat conduction to the substrate, the part becomes hotter and the temperature increases with the layer number.

The thin-walled rings with different curvatures can be handled by defining different radiuses. To show influence of different thin-walled rings' radiuses on the molten pool temperature, the molten pool temperature distribution is studied with the radius of $R=1, 2, 3, 4, 5, 6, 8, 10,$ and 15 mm when depositing the first layer. Figures 17 (a) and (b) are showing the typical temperature field distributions of the thin-walled rings with the radius of 1 and 4 mm, respectively.

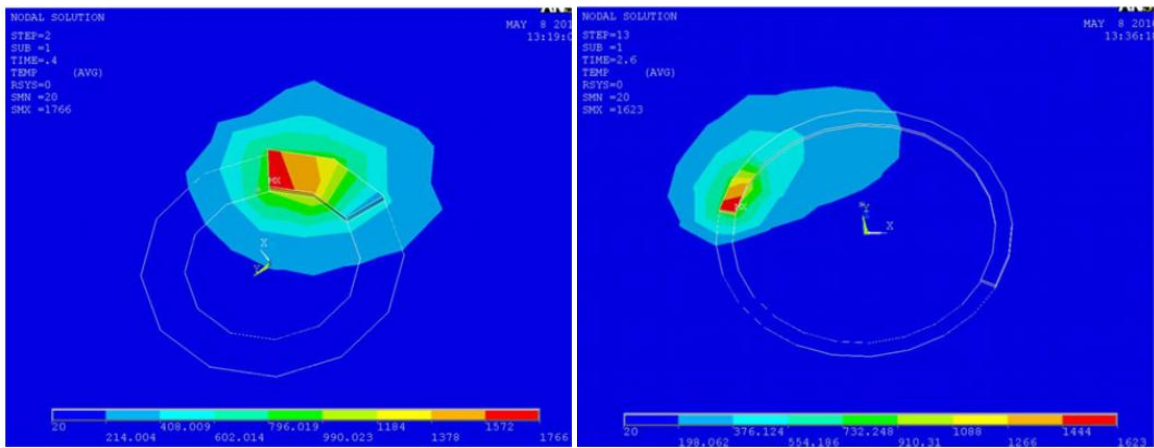


Figure 17: Temperature field distribution with different radius ^[10]

As can be seen from Figure 18 (a) (keeping power same) the molten pool temperature decreases with the radius, namely, the molten pool temperature increases with the curvature. It is also observed that the molten pool temperature tends to be gentle when the radius is more than 4 mm. This indicates that the influence of the radius on the molten pool temperature is weak when the radius is more than 4 mm. In order to keep the molten pool temperature stable for different radiuses, the trend of laser power changing can be obtained based on the $1,570^{\circ}\text{C}$ produced by temperature field computation of the thin wall's first layer. And the relationship between laser power and radius was shown in Figure 18 (b) (keeping temperature same).

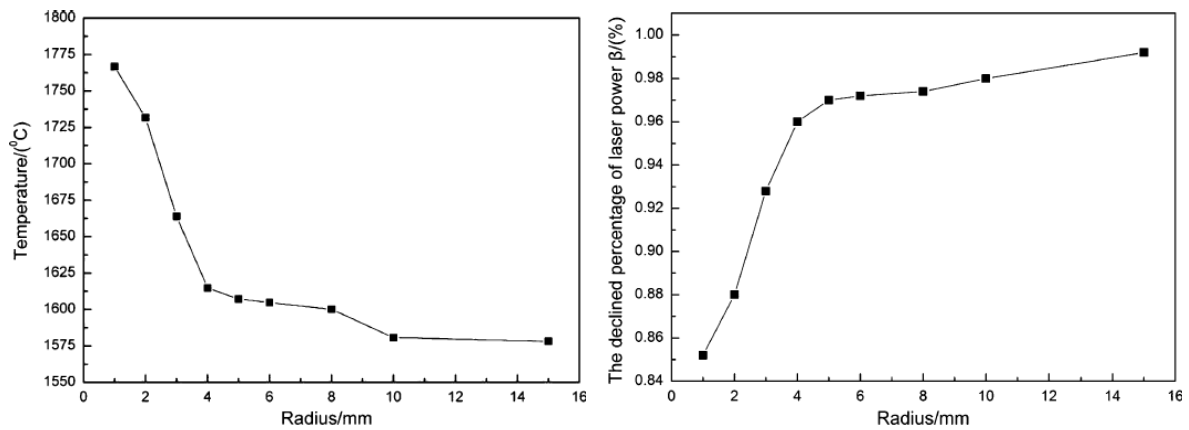


Figure 18: Relationship between temperature distribution and radius ^[10]

Layer thickness increases gradually with layer number and decreases with radius. Figure 19 (a) with constant laser power, Figure 19 (b) with varied laser power.

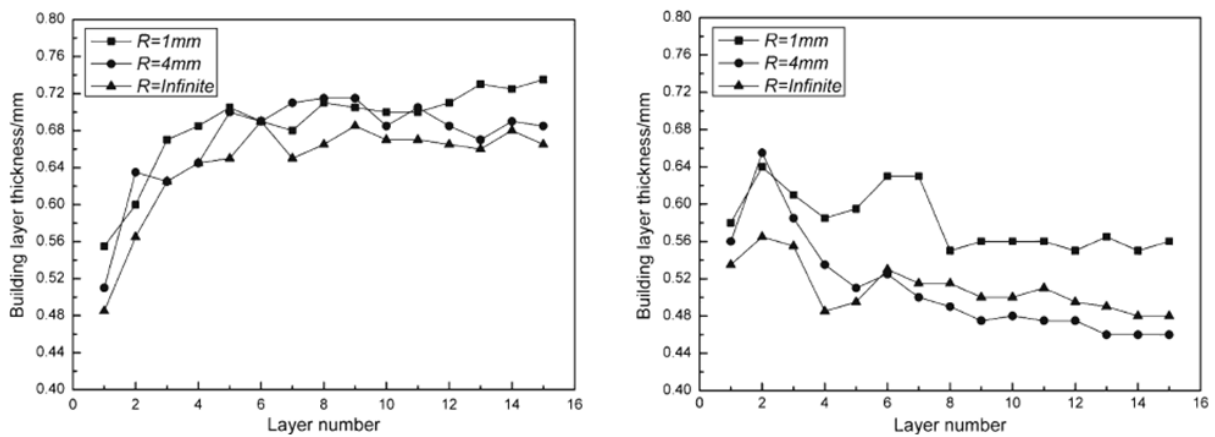


Figure 19: Relation between building thickness and layer number, (a) with constant laser power, (b) with varied laser power ^[10]

The effects of thin-walled blade's curvature change and accumulating layer number on the temperature field distribution were calculated and the trend of laser power changing with the layer number and curvature in the processing of the thin-walled blade can be obtained by simulation when keeping molten pool temperature stable. The experimental results show that the excessive build-up occurred with constant laser power because of the increase of energy density at corners and the thickness with varied laser power is more uniform than the constant laser power.

2.1 Analysis of coupled thermal (thermal plus structural)

M. Labudovic et al ^[11] create a FEM model to calculate transient temperature profiles, dimensions of fusion zone and residual stresses. Model simulations are compared with

experimental results acquired on line using an ultra-high shutter speed camera which is able to acquire well contrasted images of the molten pool, and off line using metallographic and x-ray diffraction analysis.

As a first step, a high shutter speed imaging is employed in monitoring the deposition of 100 mesh MONEL 400 alloy on AISI 1006 steel, at variety of laser power and scanning speeds. Both numerical and analytic model were developed for thermal history. Results from heat transfer analysis were then used as loads for FE analysis of residual stress and the results were compared with x-ray diffraction technique.

Assumptions:

- Work piece initially at 298K.
- Thermo-physical and mechanical properties are temp dependant.
- Beam diameter at which power density reduced by e^2
- Normal distribution.
- Latent heat of fusion is simulated by artificial increase in liquid specific heat.
- Convective heat flow is neglected.

Numerical solution to the model:

- ANSYS Parametric Design Language to provide heat boundary condition at different time.
- First iteration solve the system equation assuming starting temp 298K.
- Subsequent iteration use temp from previous iteration to calculate conductivity, specific heat matrix.
- First element positioned onto the substrate with set initial boundary condition.
- Subsequent element used results from previous steps as initial condition for each new element birth.
- Iteration continues for time period T until converged solution is achieved or dynamic equilibrium of heat exchange established.
- Study of heat transfer problem allow determination of temp distribution.

Experiment:

- 100 mesh MONEL 400 alloy on AISI 1006 steel, argon was used as shielding gas, Nd-YAG laser
- A fiber optic conducting 337nm wavelength laser
- Nitrogen pulse laser with 5ns pulse duration

- Camera with UV filter that allow light near 337nm wavelength to pass
- Due to reflection from mirror like molten pool well contrasted image obtained

Modeling results:

- Figure is showing typical analysis from 10mm/s and 600W laser power
- 1325 C isotherm represent fusion zone

Modeling results (heat transfer analysis)

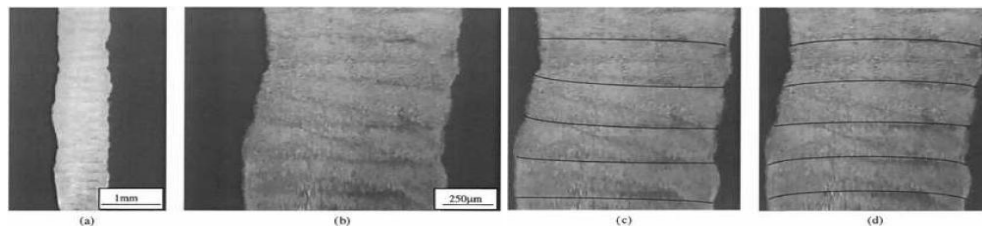


Figure 20: Micrographs of deposits^[11]

- Figure 20 shows micrograph of deposits
- a, b shows actual deposit
- c shows numerical modeling
- d shows analytic modeling

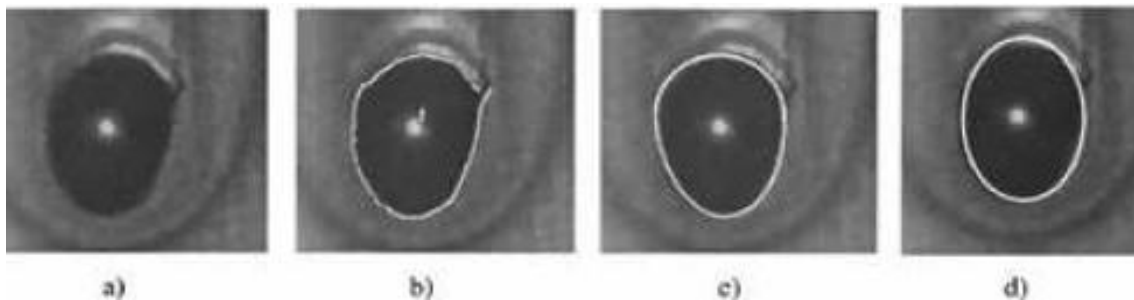


Figure 21: Comparison of melt pool boundaries obtained by the processing result of the edge detector with those obtained by the modelling, (a) original image acquired by high shutter speed camera, (b) processing result of edge detector, (c) numerical mode^[11]

- Isotherm corresponding to 1325 C.
- a, b, c, d as obtained by high shutter speed camera, edge detector, numerical and analytic modeling (Edge detection is the name for a set of mathematical methods which aim at identifying points in a digital image at which the image brightness changes sharply or, more formally, has discontinuities. The points at which image brightness changes sharply are typically organized into a set of curved line segments termed edges).
- Pool is deeper at the end than at front due to heat accumulation.
- Increase power and decrease speed widens the pool.

Stress analysis:

- Sample was allowed to cool down below 50 C between each subsequent build to eliminate preheating effect.
- Residual stress investigated with XRD (Xray diffraction technique is nondestructive analytical technique for identification and quantitative determination of various crystalline forms known as phase Identification is achieved by comparing x ray diffraction pattern Study crystal deformation and stress properties)
- Comparison was done with FE modeling.
- Compressive residual stress at the center and tensile towards the edges.
- Effect of subsequent layer is shown in the Figure 22.
- Both figures showing same distribution for 1st layer then progressive increase in tensile residual stress in subsequent layers.
- With layers deposition transverse as well as longitudinal cracks are detected due to stepwise increase in residual stress.
- Cracking can be avoided by preheating, but reduces cooling rate.

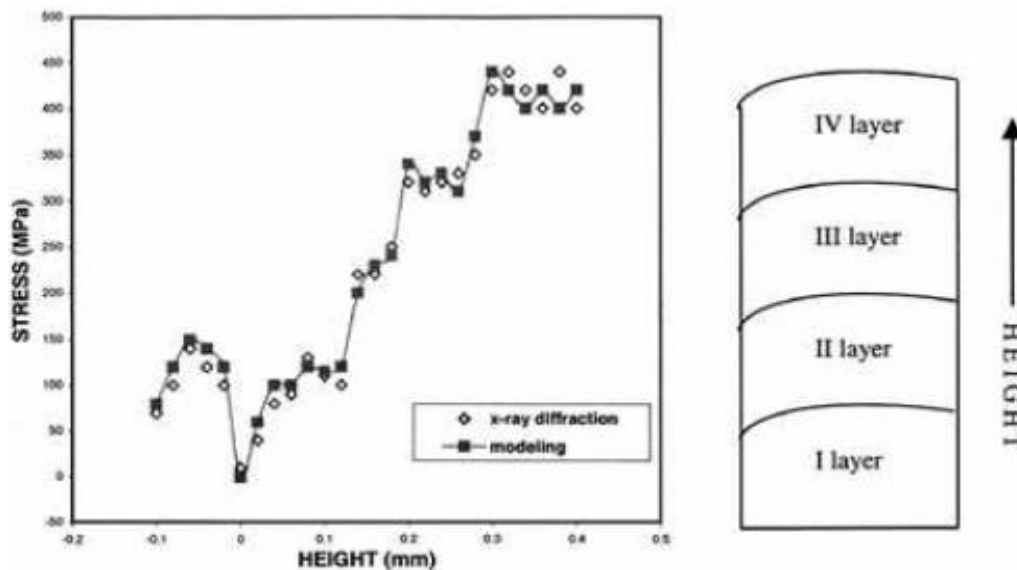


Figure 22: Distribution of residual stresses within subsequent layer, comparison between x-ray diffraction results and modelling results ^[11]

- Cracking prevention mechanism by preheating increases ductility of MONEL 400 alloy.
- Preheating treatment to 400C reduces stress to 400MPa.
- Post heating to 600C further reduces stress to 200MPa.

- Simulation gives cross sectional shape of melt pool certified by topside image by camera.
- Modeling of residual stress confirmed by X-ray diffraction residual stress measurement.

A three-step analytical and numerical approach was carried out by Peyre et al ^[12] to predict the shapes of manufactured structures and thermal loadings induced by the DMD process. First, powder temperature was calculated using a analytical model, then the geometry of walls was predicted by a combined numerical + analytical modelling, finally thermal behaviour during DMD of a titanium alloy was described.

The thermal model takes into account the moving interface during metal deposition with a specific function $\kappa(t, x, y, z)$ allowing the conductivity front to move simultaneously with the moving laser source (with an appropriate spatial energy distribution), thus representing rather precisely the DMD process. This allowed us to provide an adequate representation of temperatures near the melt-pool, and to reproduce with a good accuracy thermal cycles and melt-pool dimensions during the construction of up to 25-layer walls. This was confirmed by comparisons with experimental thermocouple data $T = f(t)$, and fast camera melt-pool recording.

Following these works, our objective was to propose a combined analytical–numerical approach, to predict geometries and thermal fields involved during a DMD process, considering only the experimental parameters such as mass feed rate D_m (g min⁻¹), laser power (W) and scanning speed V (m s⁻¹) as input data.

Experimental validation: Dedicated DMD experiments were carried out (between 1 and 8 layer), using different parameters (mass feed rate in the 1–4 g min⁻¹ regime, laser powers between 100 and 400 W), to compare with simulations results. The global agreement between experimental data and calculations is satisfactory Figure 23. Calculated widths and average deposition heights are well reproduced (15% maximum difference) by measurements carried out on cross-sections, over a rather wide range of laser and powder feeding conditions. Moreover, the simulation-aided morphological model allows describing with a reasonable agreement the evolution of geometrical parameters with the number of layers n as shown in Figure 23. Consequently, the theoretical approach seems to be accurate enough to predict the geometry of walls before performing finite element thermal simulations.

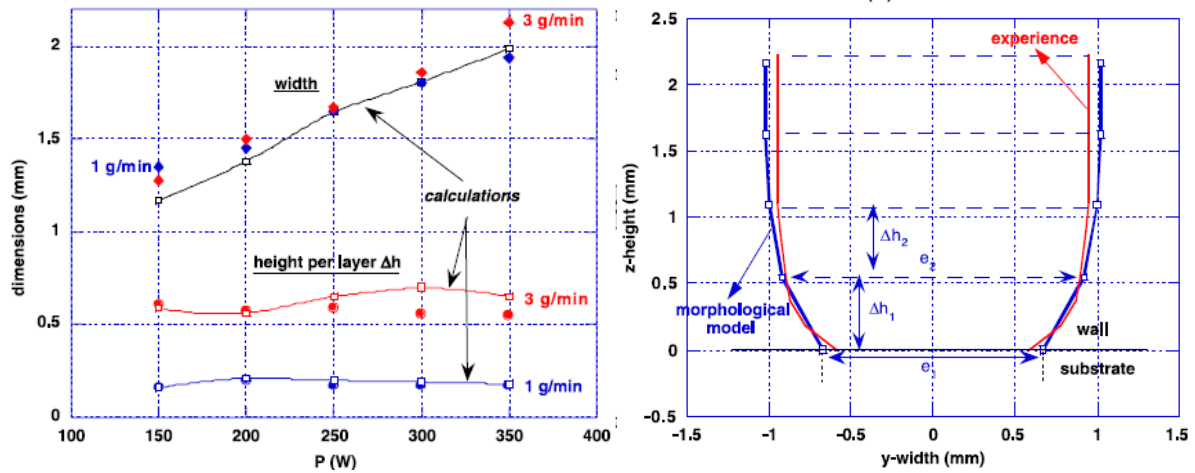


Figure 23: Comparison between experimental data and simulated values, (a) influence of laser power and mass feed rate on the stabilizing geometrical features of a DMD wall ^[12]

Experimental $T = f(t)$ profiles exhibit a quasi-sinusoidal aspect corresponding to the alternated displacement of the laser head Figure 24. With a 35% absorptive of the laser beam, it appears that COMSOL simulations allow one to reproduce rather well those temperature-time profiles recorded by thermocouples, whatever the process parameters. Thermocouple data obtained with 5 or 6 thermocouples located at various positions in the substrate, and near the wall, are systematically well reproduced. This is particularly true concerning the global thermal chronology, but also for the first $T = f(t)$ peak corresponding to the first layer, and for all the following peaks corresponding to the 2nd , 3rd . . . layers Figures 24(a) and (b). This has been confirmed for various mass feed rates Dm ($g \text{ min}^{-1}$), various scanning speeds V ($m \text{ s}^{-1}$) and various laser powers P (W), for a unique 0.35 absorptive value.

We can also obtain local temperature versus time data into the wall Figure 24 (c), and deduce numerically heating and cooling rates, together with the tempering temperature which corresponds to the average temperature achieved in the wall after a long manufacturing time. Melt-pool sizes (length and height) are slightly overestimated by simulations. The melt-pool enlargement is due to lower heat dissipation far from the substrate and contributes to wider walls until the melt pool reaches a stabilized value

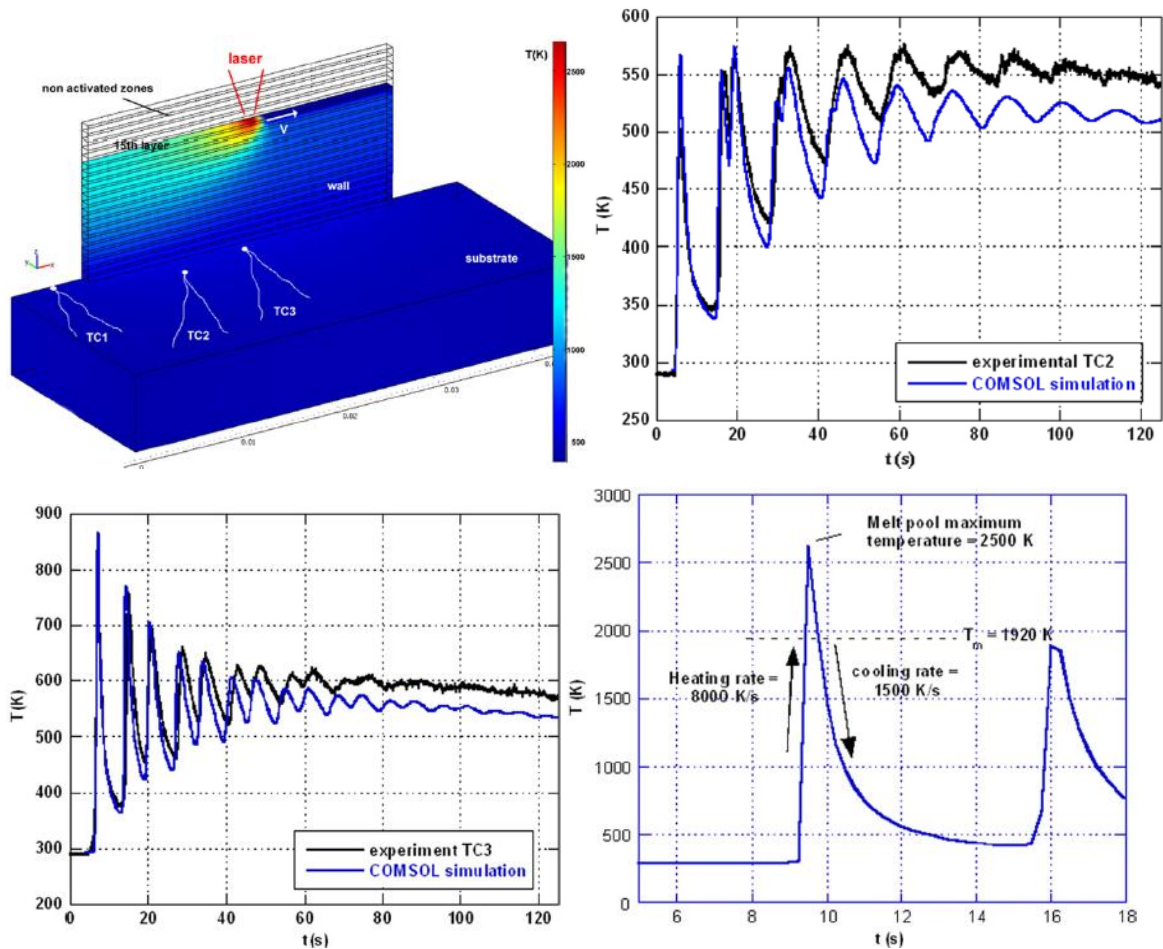


Figure 24: Comparison between experimental and simulated profiles (600 W, 0.006m/s), (a) thermocouple TC2, (b) TC3 (c) Temperature versus time simulated in the middle of the wall ^[12]

This DMD global model has already been successfully applied and validated on other aeronautical alloys such as Inconel 718 or Rene 142.

The process of DMD involves very high thermal gradients and heating and cooling rates, resulting in residual stresses and distortion, Heng Liu et al ^[13] presented a thermo-mechanical finite element model to predict residual stress and deformations. The thermal distribution, thermal stress field, geometry deformation and effect of deposition parameters on residual stress and deflections are explained.

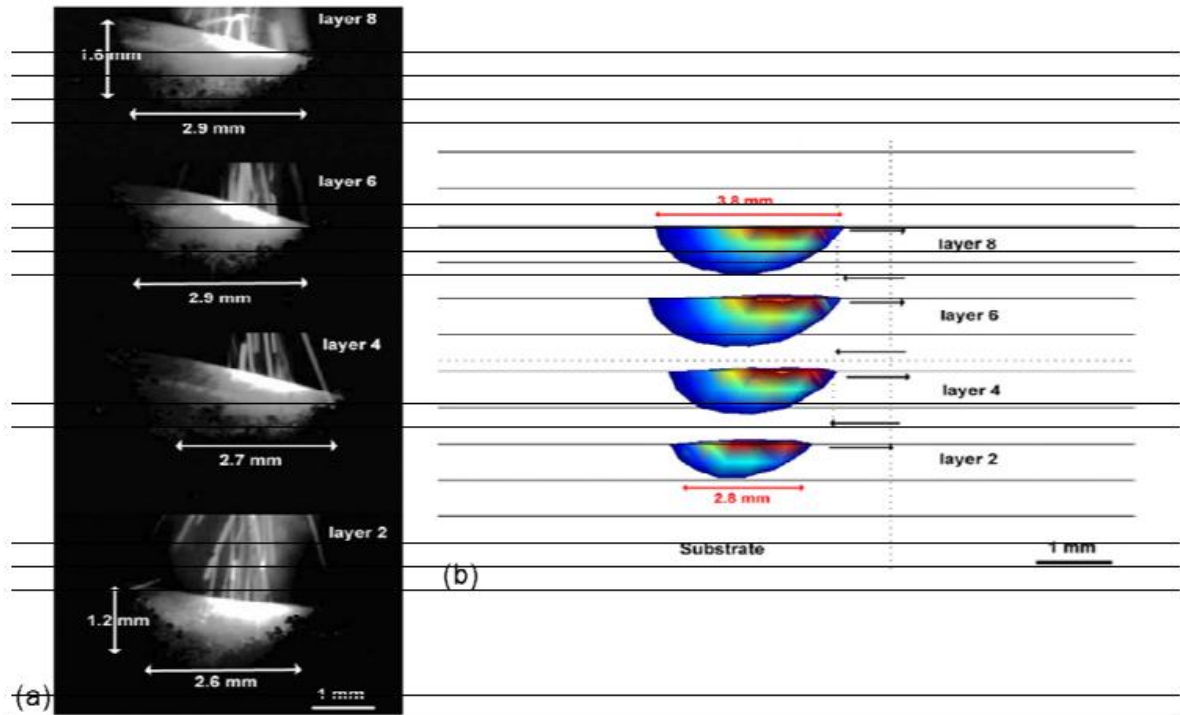


Figure 25: Comparison between (a) experimental (1000 Hz C-Mos fast camera), (b) simulated laser induced melt pool (600W, 0.006 m/s), between 2nd and 8th manufactured layers ^[12]

(a)

(b)

Normal and Von-Mises stress at top and bottom are shown in Figure 26 (a) and (b).

Unlike most of the analysis the workpiece is fixed from the left side and deposition is added up at the centre area.

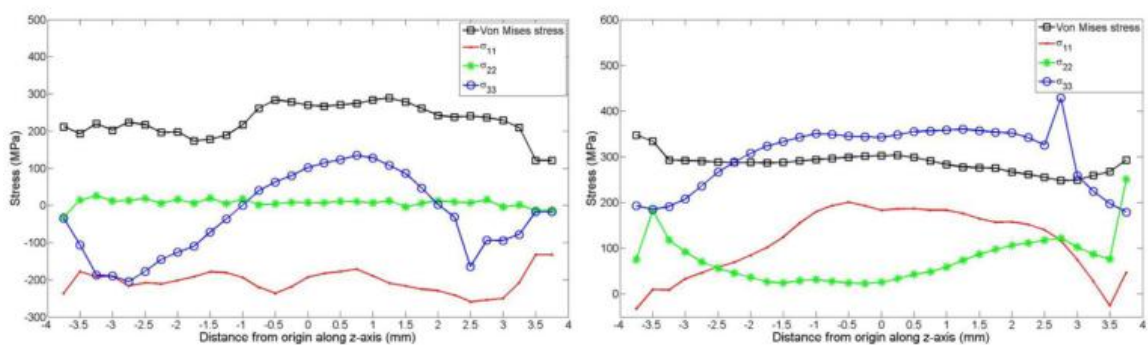


Figure 26: Residual stress on (a) top surface, (b) bottom surface of deposit along z direction ^[13]

(a)

(b)

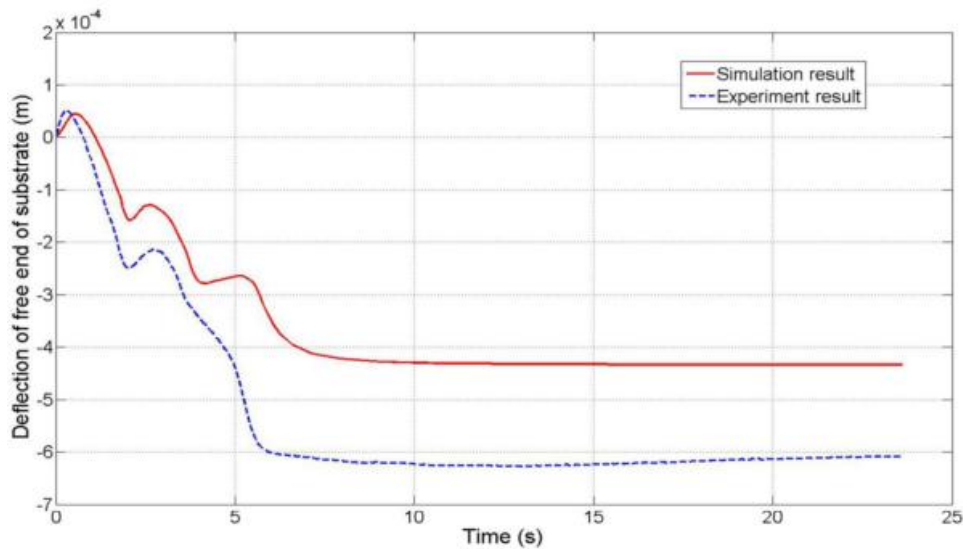


Figure 27: Simulation and experimental results of deflection of substrate ^[13]

In the plot of Figure 27 the trend of deflection first bend down due to thermal expansion on the top surface and then bend up during the cooling process, after completely cool down substrate keeps the deformed shape.

Verma and Shukla presented LMD thermal analysis using Ansys Parametric Design Language (APDL) based FEM to simulate a moving heat source for SS316 and Ni [14]. The overall conclusions derived from an in-depth literature review are listed in ^[15]. Shukla and Verma modelled different cases and numerically analysed the LDMD process^[16].

4.2 Conclusion from literature review

1. As the layers increases cooling rate decreases towards the top layers.
2. At the bottom of the molten pool temperature gradient is high and cooling rate is small.
3. From bottom to the top of the melting pool, temperature gradient along X axis (horizontal axis) increases gradually and the component of Z axis (vertical axis) decrease gradually. As the layers increases the thermal gradient along the horizontal exceeds that of the vertical direction.
4. The peak temperature experienced by a particular layer gradually reduces as the laser beam moves to the higher layer.

5. Deposited layers undergo high cooling rate which is particularly at its highest at the solid-liquid interface and decreasing with the increasing distance from the centre of the melt pool.
6. With the increase in build height, the heat loss towards the substrate is reduced, and thus, heat input per unit length needs to be reduced to avoid over-melting along the top layers.
7. Laser power, scanning velocity, powder mass flow rate, and idle time between the deposits of successive layers influence the thermal behaviour induced in the deposited material.
8. Thermal history of the deposited material at different locations has the same changing trend.
9. During the initial stage, the deposited material experience a quenching effect and can attain a very high cooling rate. Then the peak temperature of thermal cycle decreases and even disappear and the resident temperature increases continually as the subsequent layer atop it increases.
10. For constant laser power and scanning speed, the layer width and peak temperature increases while the cooling rate decreases towards the top layers.
11. Solidified deposit has cellular structure with increase in cell spacing as the cooling rate reduces towards the top layers.
12. Too higher scanning speed will result in a poor bonding strength and higher sensitivity of cracking, appropriate scanning speed should be used in order to obtain better forming qualities.
13. Excessive build up occurred with constant laser power because of the increase of energy density at corners and high curvatures and thickness with varied laser power (keeping temperature same) is more uniform than constant laser power.
14. Molten pool developed during the process is deeper at the end than at the beginning because of the heat accumulation.
15. In comparison with single layer, subsequent layer built result in an increase in residual stresses.
16. Cracking may occur laterally or longitudinally. Cracking can be avoided by preheating the specimen.

2.4 Problem Formulation and Gap Identification

While going through the literature review it is found that many researcher had used different different type of laser beam and done the analysis on different type of commercially available software like ABAQUS, ANSYS, COMSOL. And found out the peak temperature with respect to the time and distance by varying many parameters like laser power, feed rate of material, velocity of movement of laser beam. Like et al Jia Yang & Fude Wang⁽⁴⁾ had done the study of Gaussian laser beam distribution and found out the temperature at two different position such as first is at just below the layer where the laser has started the operation and second at some where middle to the subject structure and found out the peak temperature of the subject which come near about 1888K but comparison of the beam is missing in the papers and not found anywhere. Which is a huge problem as if anyone want a particular temperature at any point than so that the microstructure of the subject can be judge easily and desired properties can be achieved easily there is no paper which will give them knowledge about this topic to do. In our study by using commercially used ANSYS 14.0 the difference between the material under same parameters but different type of laser beam is carried out by using couple thermal analysis.

CHAPTER 3 Methodology

3.1 Structure analysis

For explaining the structural analysis I am explaining an example of the bicycle frame shown in the following figure. The frame is to be built of hollow aluminium tubing having an outside diameter of 25mm and a wall thickness of 2mm for the main part of the frame. For the rear forks, the tubing will be 12mm outside diameter and 1mm wall thickness.

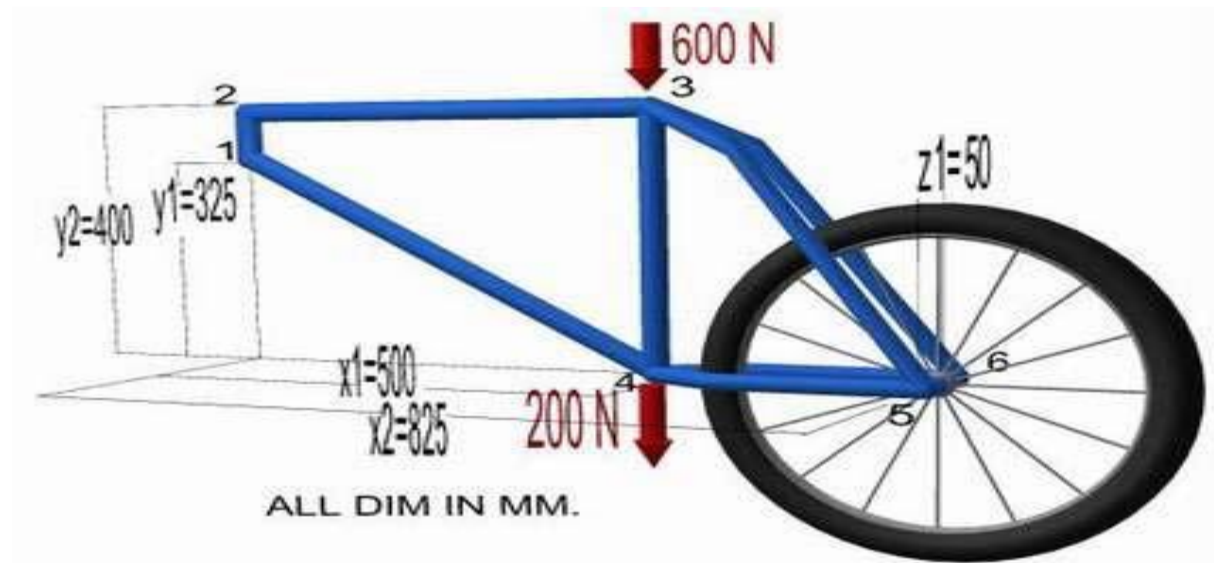


Figure 28 Model of bicycle

```
/title,3D Bicycle Space Frame
```

```
! for titling the file name
```

```
/prep7
```

```
! this command will enter into pre-processor
```

! Define Some Parameters, these parameter is not needed to be define but by defining these parameters we will have the freedom to change the frames by just defining the values again

```
x1 = 500
```

```
x2 = 825
```

```
y1 = 325
```

```
y2 = 400
```

```
z1 = 50
```

!In below command we will define the key points for the frame of the bicycle and the general command should be

! k,key-point number,x-coord,y-coord,z-coord

K,1, 0,y1, 0

K,2, 0,y2, 0

K,3,x1,y2, 0

K,4,x1, 0, 0

K,5,x2, 0, z1

K,6,x2, 0,-z1

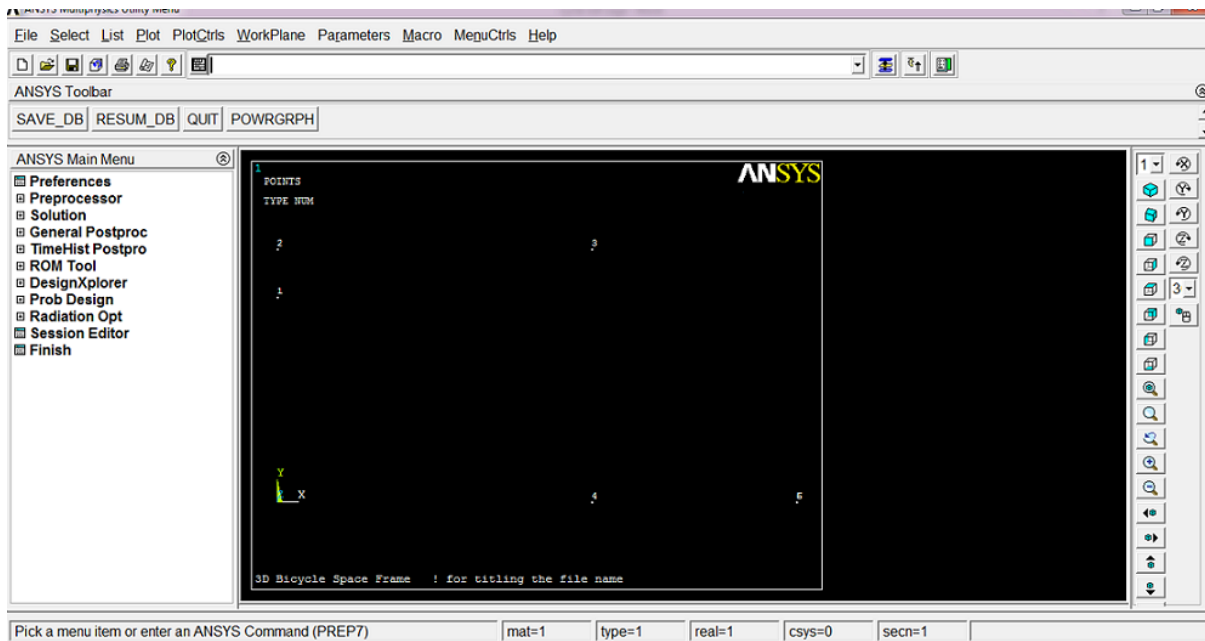


Figure 29 keypoints of model

! by the below command we will join two key points by a line

! l,keypoint1,keypoint2

L,1,2

L,2,3

L,3,4

L,4,1

L,4,6

L,4,5

L,3,5 ! These last two line are for the rear forks

L,3,6

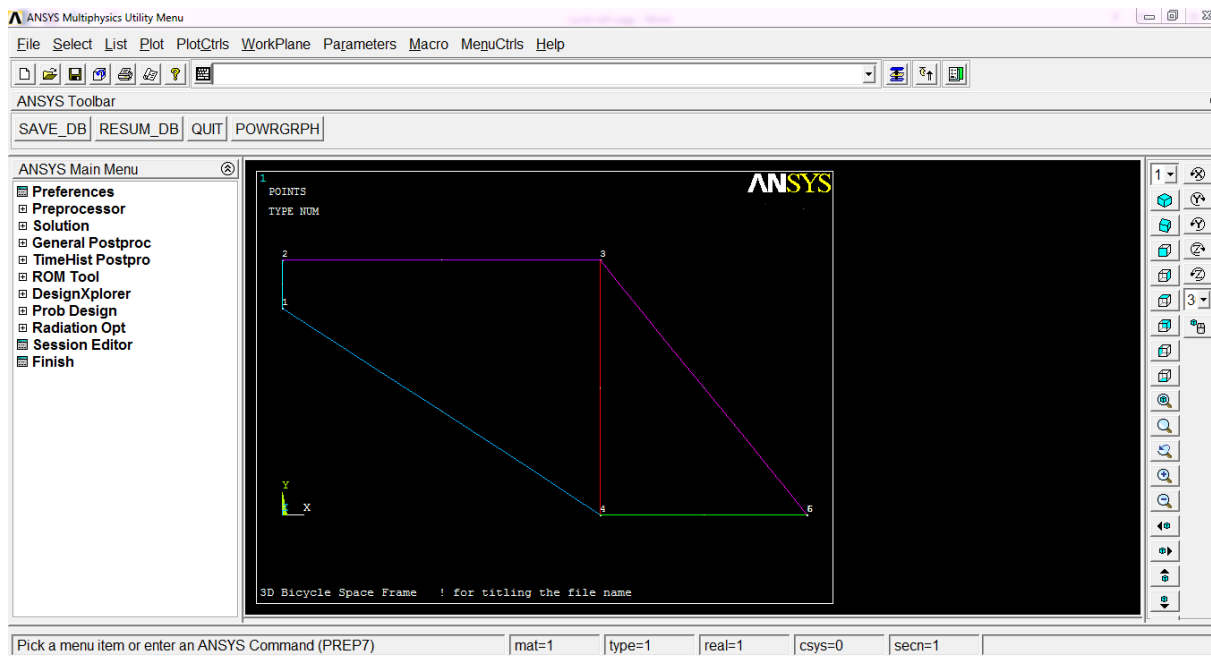


Figure 30 Line model by keypoints

! by the next command we will define the element and for the bicycle we need pipe as a element

! Define Element Type

ET,1,pipe16

KEYOPT,1,6,1

! Next command is for Define Real Constants like outside diameter inside diameter and all

! r,real set number,outside diameter,wall thickness

R,1,25,2

! Second set of real constants - for rear forks

R,2,12,1

! Next command is for Define Material Properties like Young's modulus, Poisson's ratio

! MP,Young's modulus,material number,value

MP,EX,1,70000

! mp,Poisson's ratio,material number,value

MP,PRXY,1,0.33

! now for meshing the line we have to divide the line into number of elements

! lesize,line number(all lines),size of element

LESIZE,ALL,20

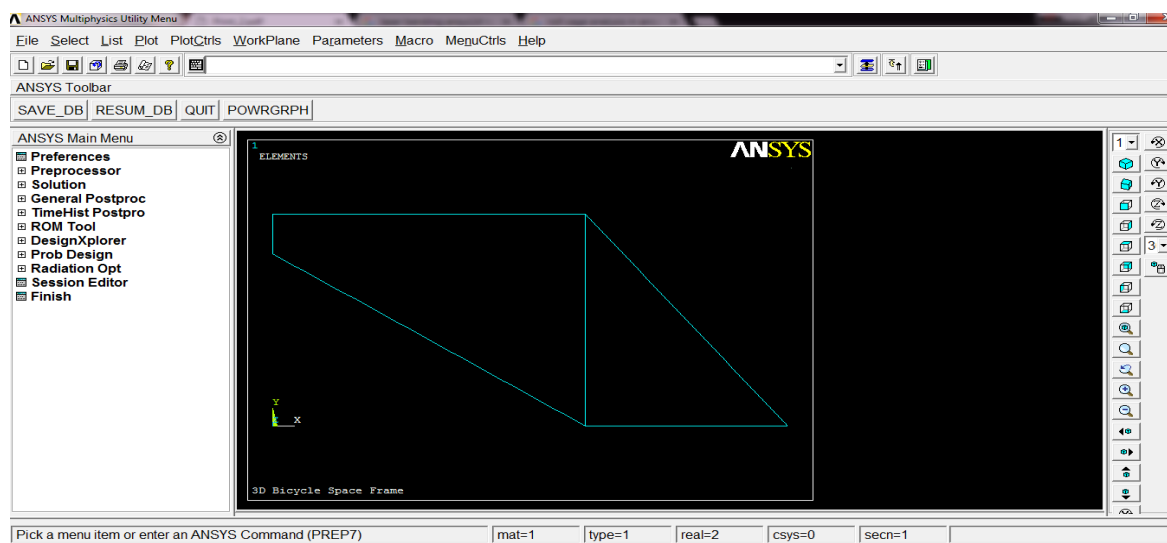


Figure 31 Meshed model of bicycle

! Now the divided lines is to be meshed for that Line Meshing is used

REAL,1

LMESH,1,6,1

REAL,2

LMESH,7,8

! Finish pre-processing

FINISH

! Enter the solution processor for solutions

/SOLU

! Analysis type,static

ANTYPE,0

! for defining displacement Constraints on Key points

! dk,keypoint,direction,displacement,,direction,direction

DK,1,UX,0,,UY,UZ

DK,5,UY,0,,UZ

DK,6,UY,0,,UZ

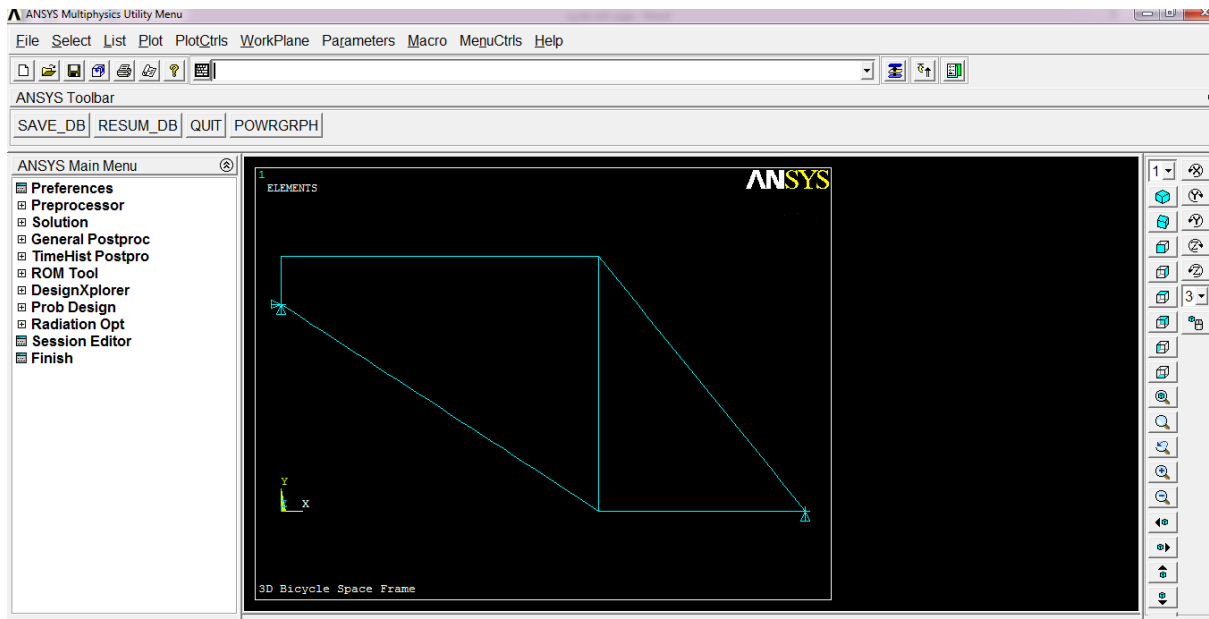


Figure 32 Model with load and constraints

! Next command will define Forces on Keypoints

!fk,keypoint,direction,force

FK,3,FY,-600

FK,4,FY,-200

! Solve the problem and finish the data entering

SOLVE

FINISH

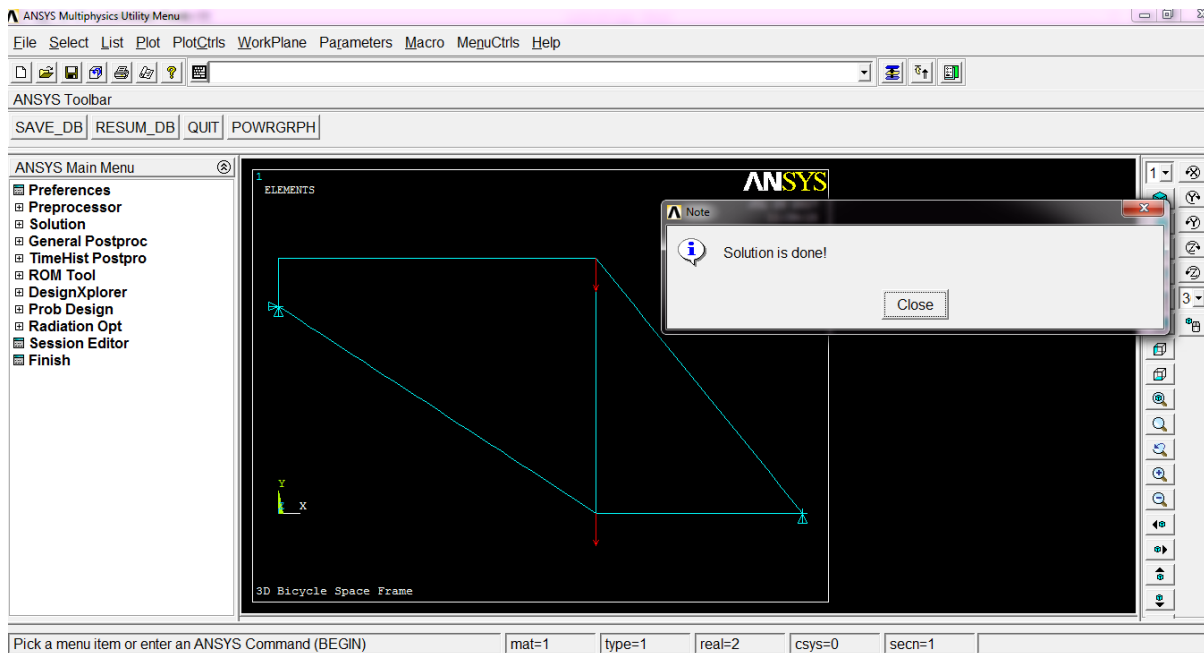


Figure 33 Solution of model

! the next command will enter the general post processor and Plot the deformed and undeformed edge

```
/post1
```

```
/WIND,ALL,OFF
```

```
/WIND,1,LTOP
```

```
/WIND,2,RTOP
```

```
/WIND,3,LBOT
```

```
/WIND,4,RBOT
```

```
GPLOT
```

```
/GCMD,1, PLDISP,2
```

```
/GCMD,2, PLNSOL,U,SUM,0,1
```

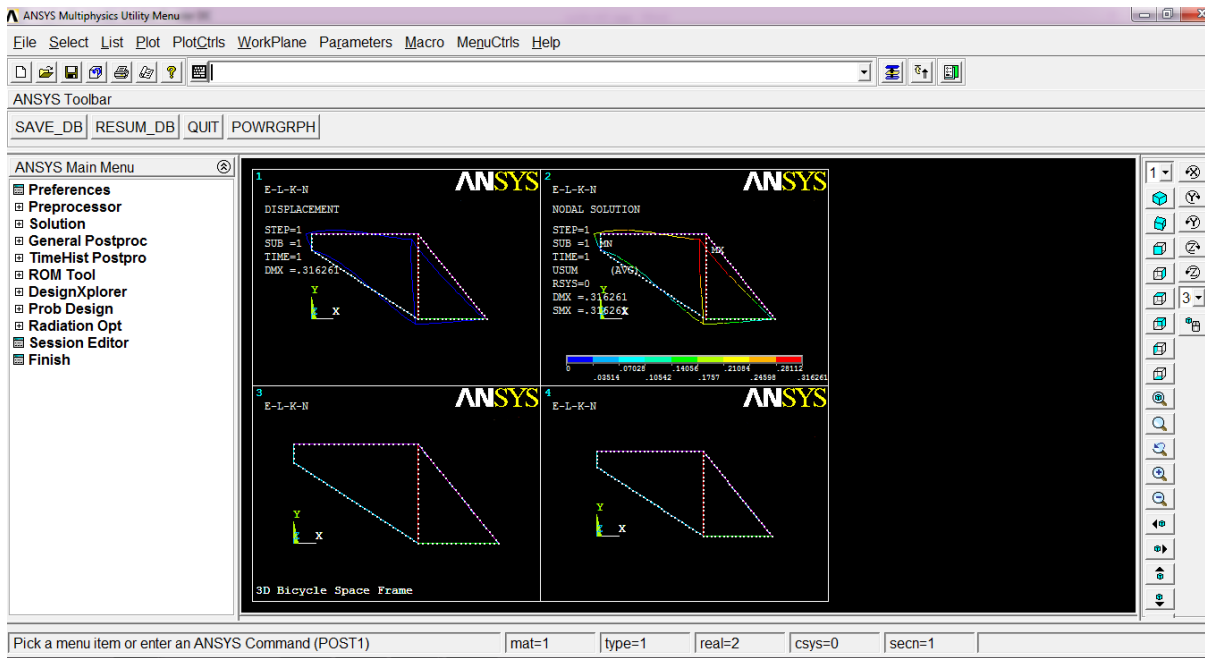


Figure 34 Deflection and real model

!For getting the results we can use the following command which will give us the stress in the bicycle

```
/GCMD,3, PLLS,vonmi0,vonmj0
```

```
/GCMD,4, PLLS,axii0,axij0
```

```
/CONT,2,9,0,,0.27
```

```
/CONT,3,9,0,,18
```

```
/CONT,4,9,-18,,18
```

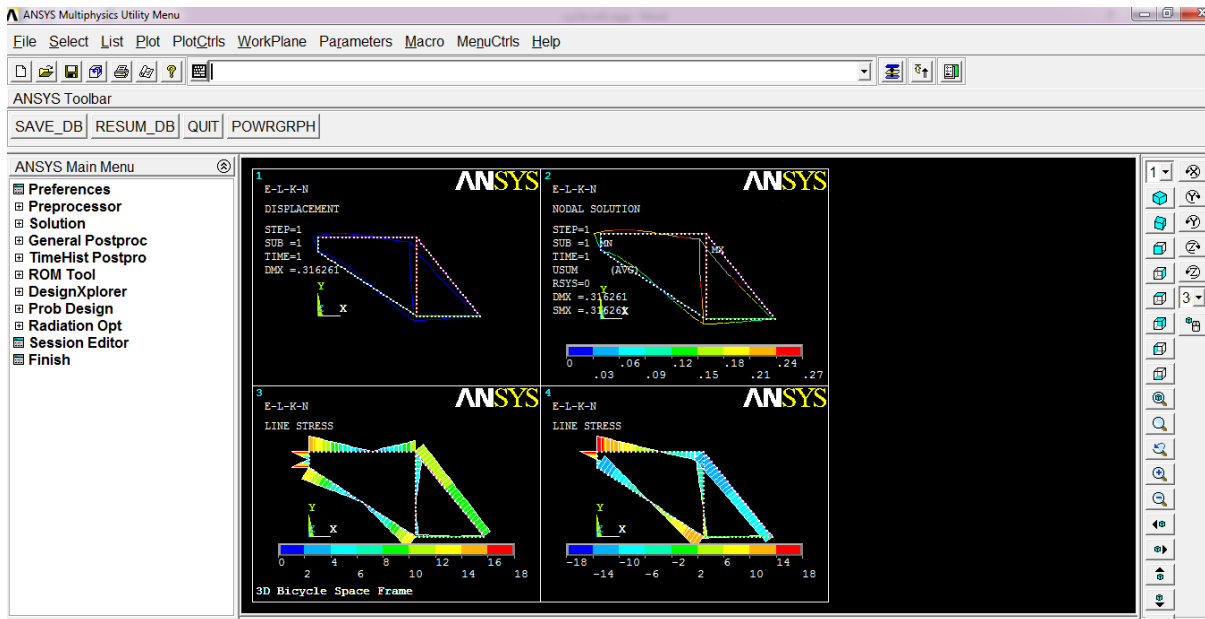


Figure 35 Stress analysis of model

3.2 Thermal analysis

For doing thermal analysis Select preferences and then select thermal in it.

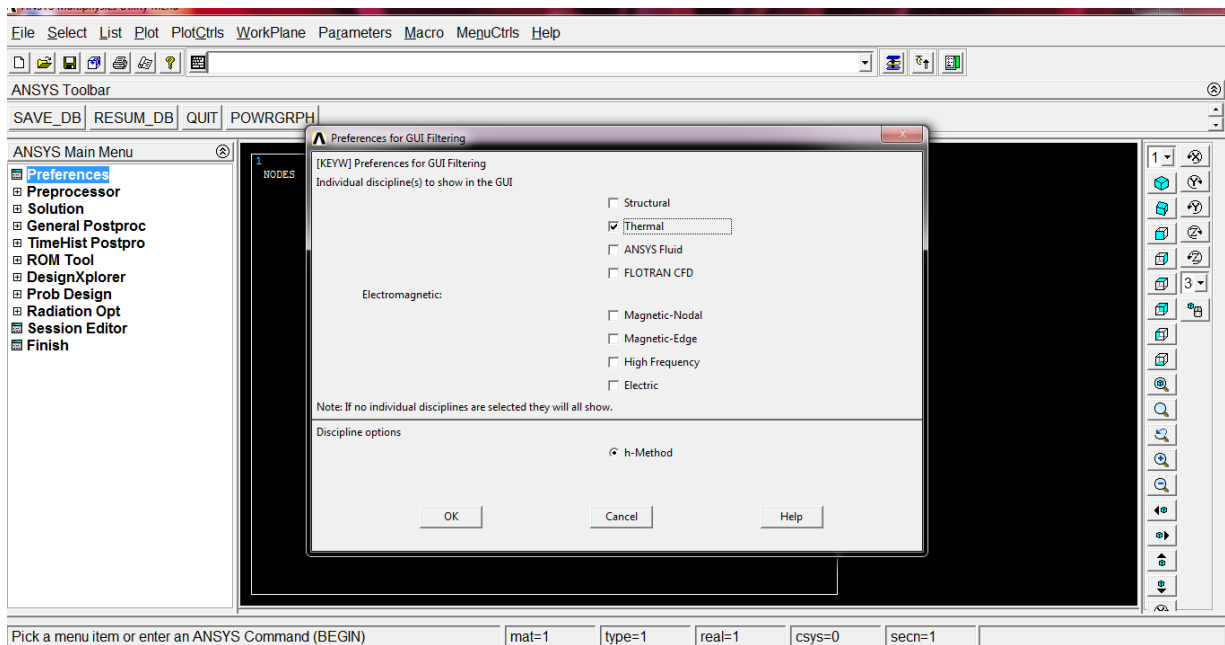


Figure 36 Pre-processor

Then for defining the element come to pre-processor and define element and then select solid plane 77 in 8 node, (square shape element). This element does not required any real constant to define.

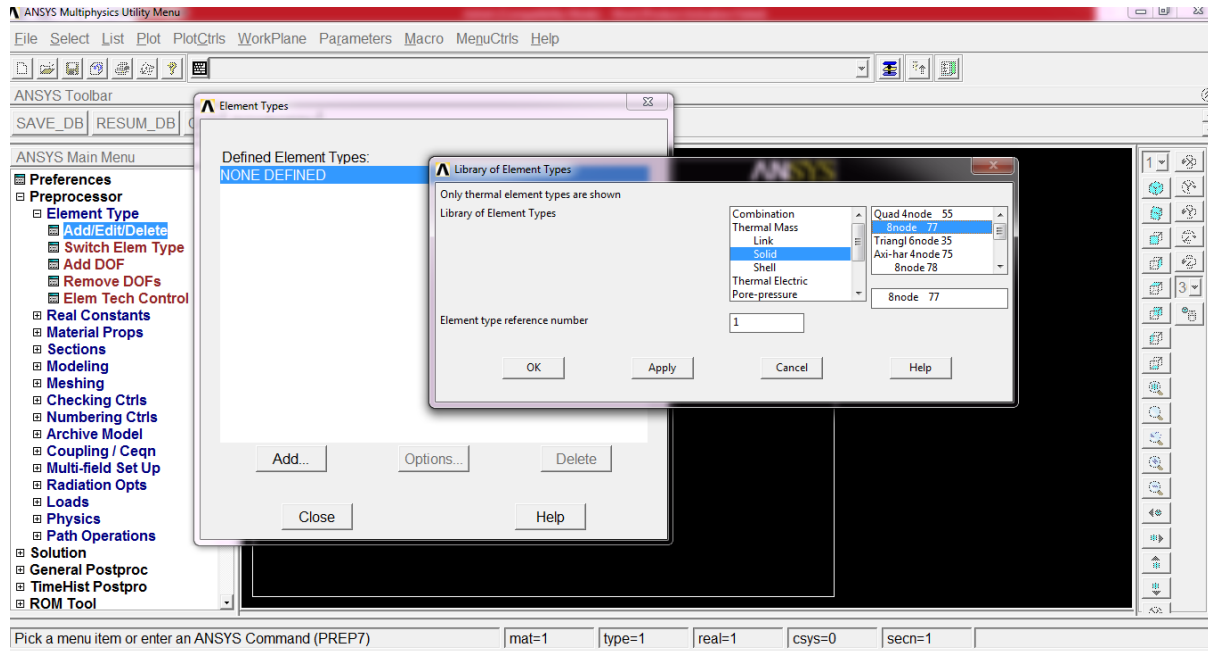


Figure 37 Selection of Element

Then for defining the material property come to material property select material model then thermal than for defining the conductivity click on isotropic give its value to be 100.

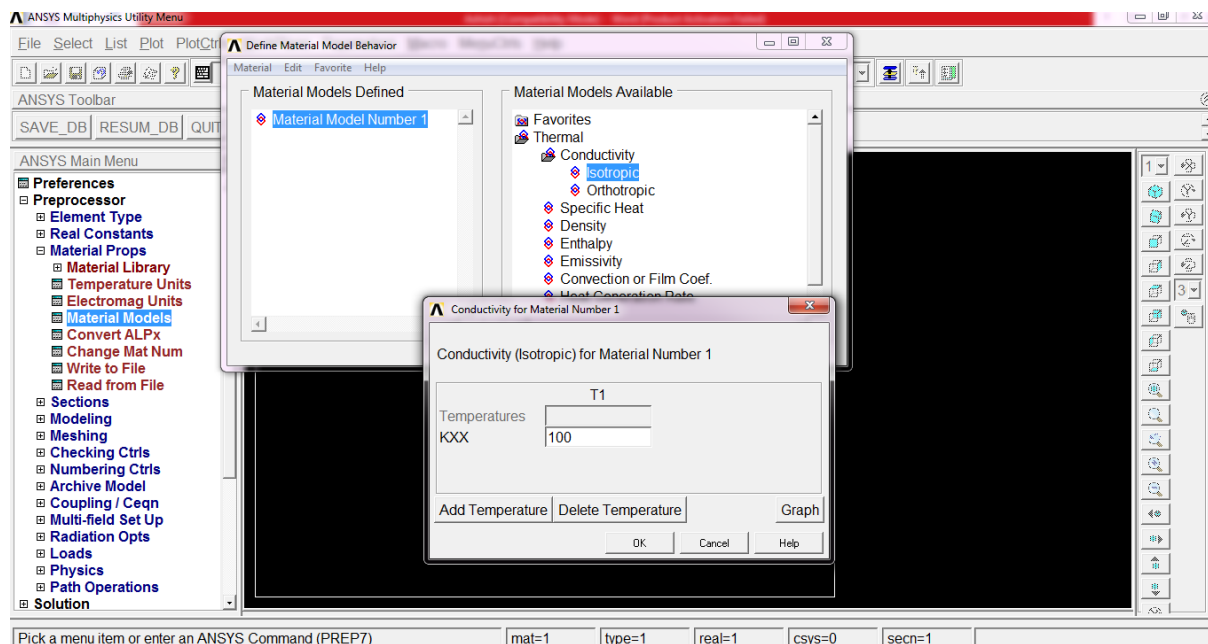


Figure 38 Material properties

Then for creating the models come to modelling section click on create then area in area we come to rectangle, by dimension we create a rectangle by giving starting point (-0.5), and ending point(0.5), in y axis starting point(-10) and ending point(10).

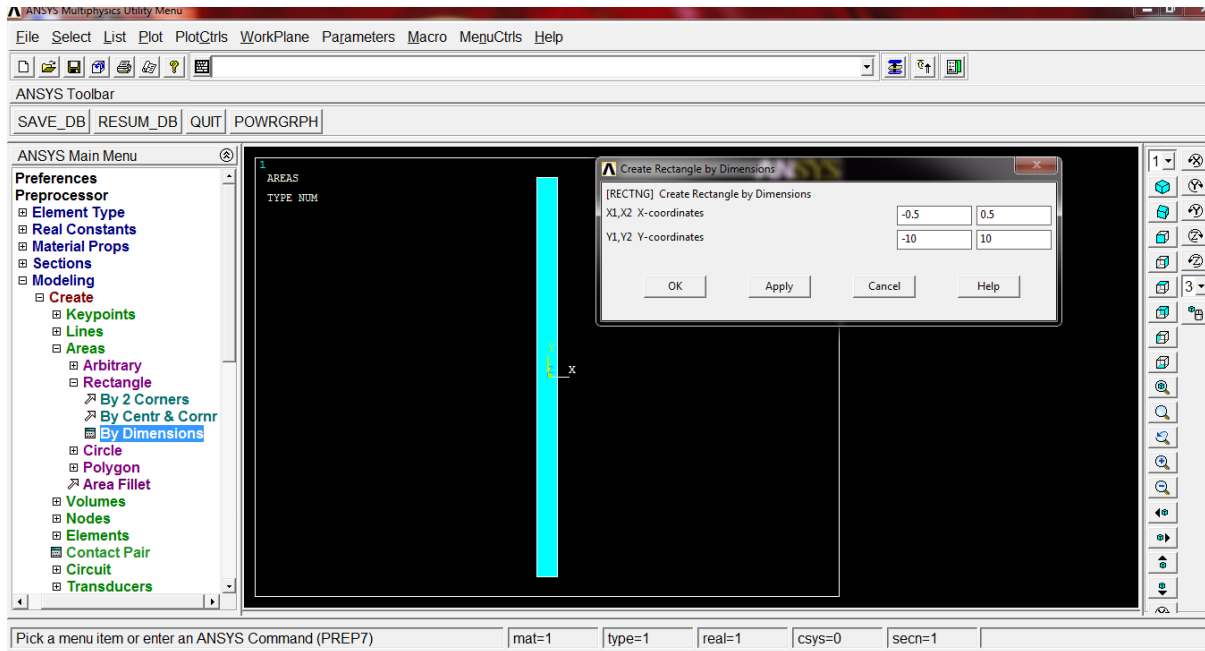


Figure 39 Rectangle model

Then for meshing the above generated rectangle use the mesh tool, then smart mesh select size 4 and then select area to be mesh and click OK and area will be meshed.

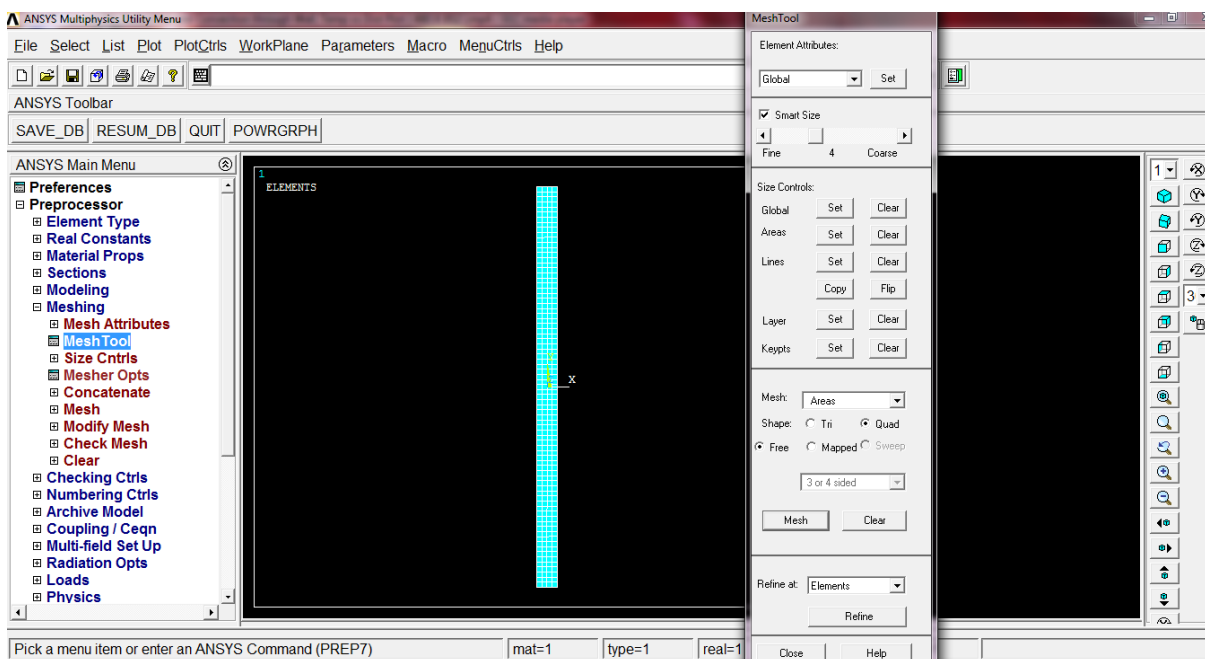


Figure 40 Meshed model

Then for applying the load, do confirm that the analysis is steady-state analysis and then define load, in thermal load apply a constant temperature on initial boundary to be 60°C.

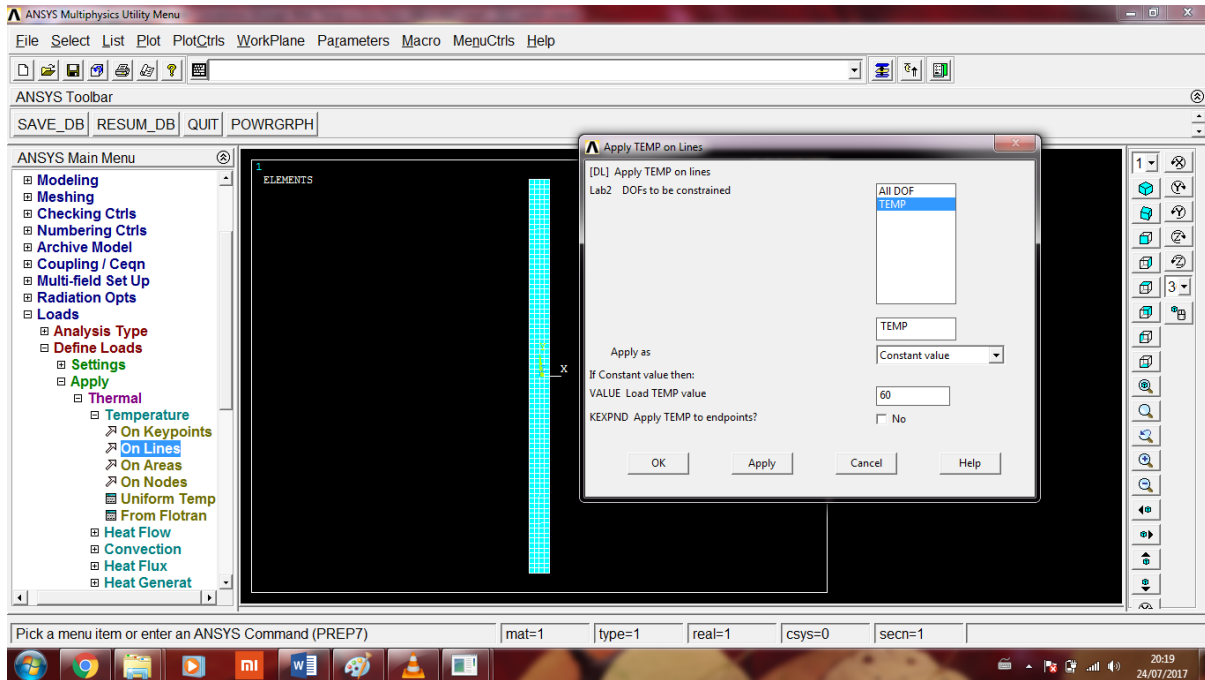


Figure 41 Convection coefficient

Then for Convection heat transfer select the final boundary line, give film coefficient to be 20, bulk temperature to be 30°C.

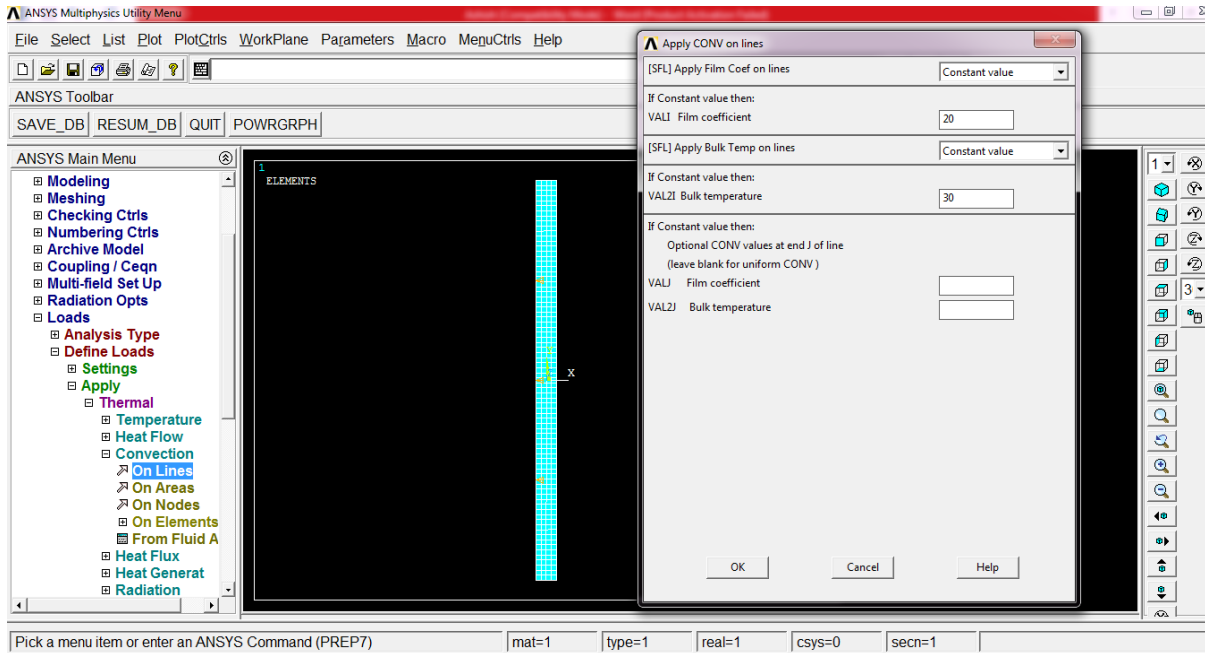


Figure 42 Boundary conditions

For avoiding the heat flux loss from top and bottom of the rectangle we will fix that surfaces flux losses to be zero.

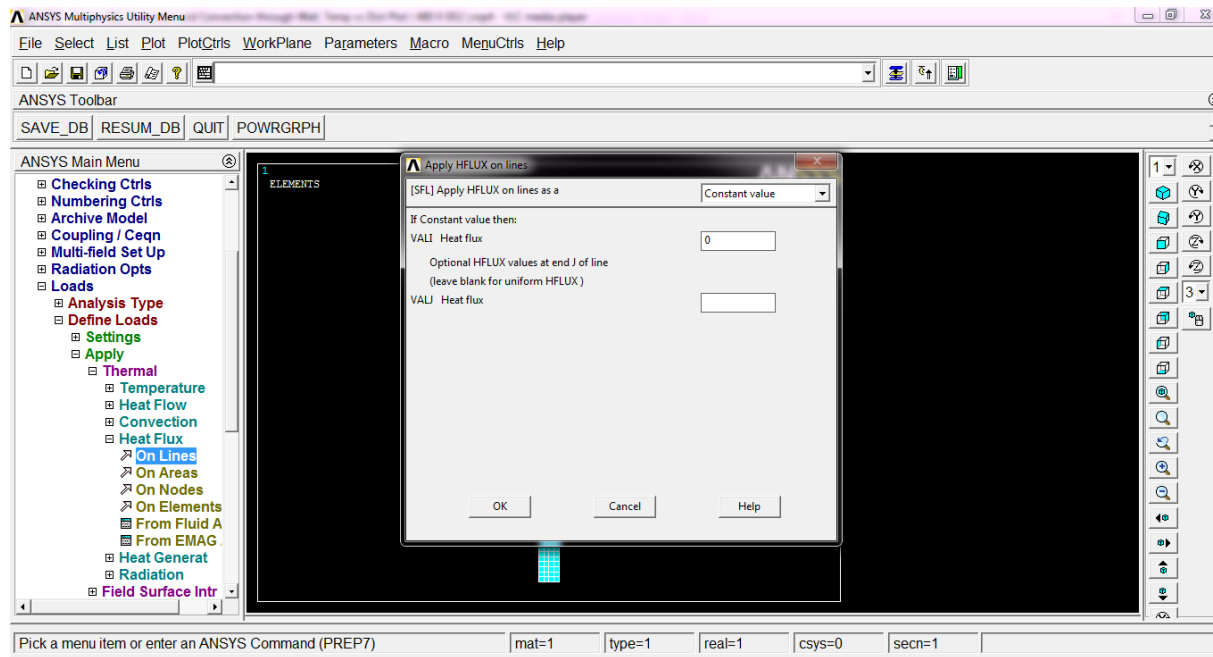


Figure 43 Heat flux condition

Solve the current model

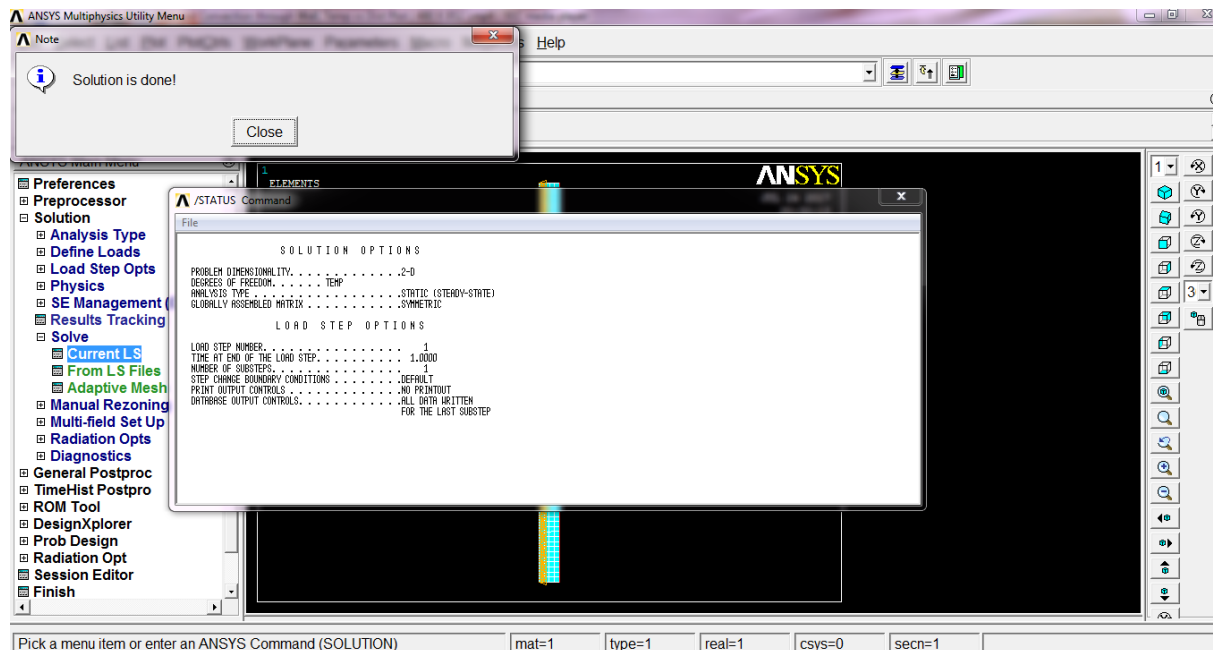


Figure 44 Solution

For getting the result of the analysis go to general postprocessor and click on plot result and contour plots and nodal solution can be seen where temperature distribution can be seen. By

which we can conclude that for this analysis min temperature is 55°C towards the end boundary line and maximum is 60°C towards the initial boundary line.

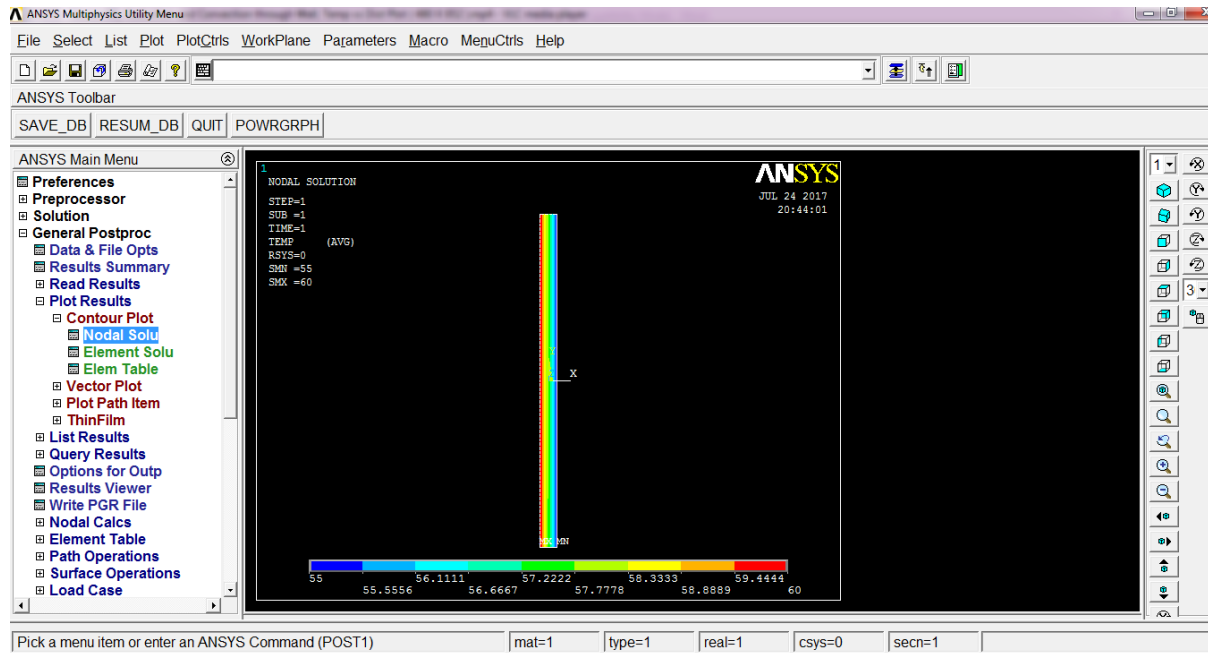


Figure 45 Thermal results

3.3 Combine (Multi-physics couple thermal analysis)

This experiment will show thermo couple example on ANSYS 14.0 The purpose of this is to outline a simple coupled thermal/structural analysis. A steel link, with no internal stresses, is pinned between two solid structures at a reference temperature of 0°C (273 K). One of the solid structures is heated to a temperature of 75°C (348 K). As heat is transferred from the solid structure into the link, the link will attempt to expand. However, since it is pinned this cannot occur and as such, stress is created in the link. A steady-state solution of the resulting stress will be found to simplify the analysis. Loads will not be applied to the link, only a temperature change of 75°C. The link is steel with a modulus of elasticity of 200 GPa, a thermal conductivity of 60.5 W/m-K and a thermal expansion coefficient of $12 \times 10^{-6} /K$.

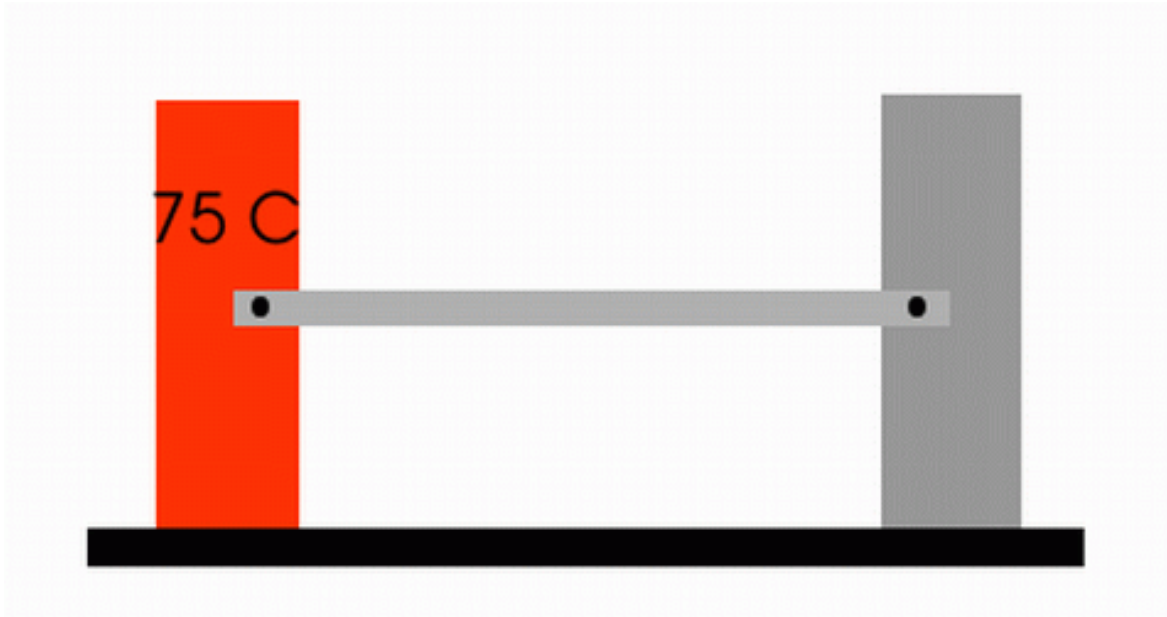


Figure 46 model of thermo couple

This command will title the file name as thermal stress

```
/title, Thermal Stress
```

```
!for Entering pre-processor
```

```
/prep7
```

```
! this command will define the key point for the middle rod
```

```
k,1,0,0
```

```
k,2,1,0
```

```
! for drawing Line connecting keypoints
```

```
l,1,2
```

```
!This command will define element type
```

```
et,1,link33
```

```
! This command will give area
```

```
r,1,4e-4,
```

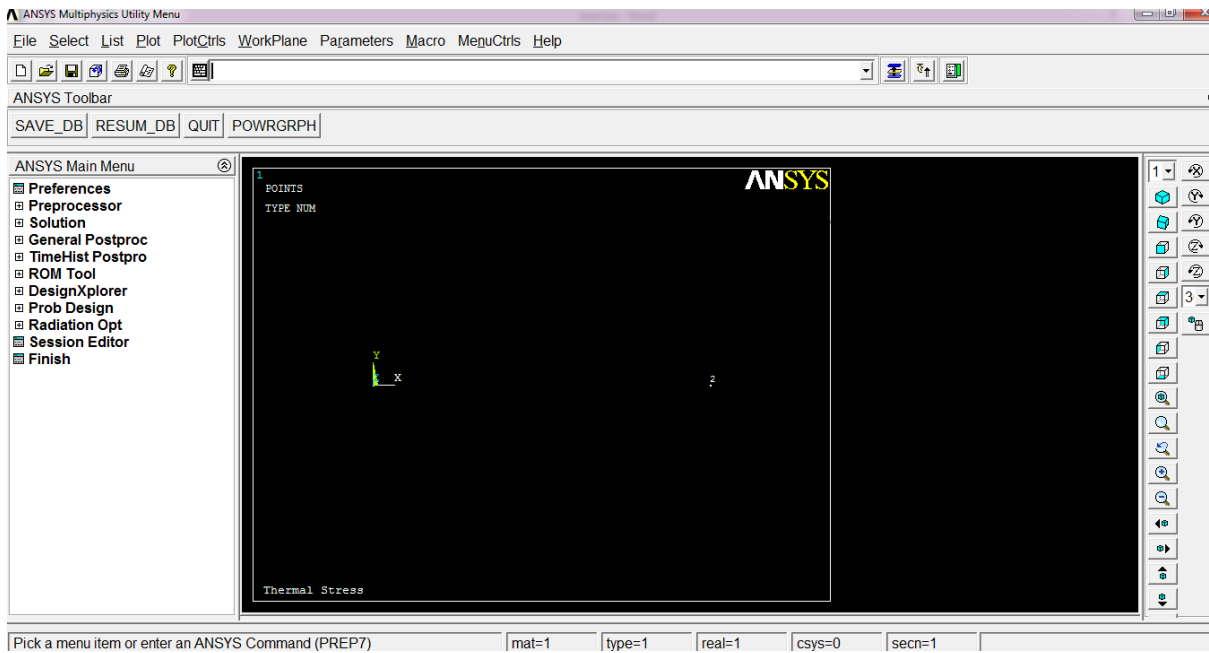


Figure 47 Node of the model

! This command will define the thermal conductivity in x axis

mp,kxx,1,60.5

!This command will give the element size

esize,0.1

! This command will the mesh above line

lmesh,all

! This command will write physics environment (working environment) as thermal

physics,write,thermal

! For entering in the new environment (i.e structural) clear the environment

physics,clear

!for defining the structural analysis element type

etchg,tts

! This command will define Young's modulus

mp,ex,1,200e9

! This command will define Poisson's ratio

```
mp,prxy,1,0.3
```

! This command will define Expansion coefficient

```
mp,alpx,1,12e-6
```

! This command will define the above properties into structural analysis

```
physics,write,struct
```

! This command will Clear the environment(i.e structural analysis

```
physics,clear
```

! This command will finish the command

```
Finish
```

! This command will enter in the solution phase

```
/solu
```

! This command will confirm that only Static analysis is in operation

```
antype,0
```

! This command will read the results in the thermal environment

```
physics,read,thermal
```

! For Apply a temp of 75°C(348K) to keypoint 1

```
dk,1,temp,348
```

! For commanding ansys to solve the problem

```
solve
```

```
finish
```

! For Re-enter the solution phase for doing the analysis in structural environment

```
/solu
```

```
physics,read,struct
```

```
! Applying loads derived from thermal environment
```

```
ldread,temp,,,,,rth
```

```
tref,273
```

```
! This command will apply structural constraints
```

```
dk,1,all,0
```

```
dk,2,UX,0
```

```
! this will solve the above command and finish the solution
```

```
solve
```

```
finish
```

```
! This will enter postprocessor, create an element table for link stress & print the element table
```

```
/post1
```

```
etable,CompStress,LS,1
```

```
PRETAB,CompStress
```

3.4 comparison between intensity distributions

In this work we had compared two basic type of laser beam they are Gaussian beam and frustum beam. For validating the results we had taken the help of “3D finite element temperature field modelling for direct laser fabrication” et.al Jia Yang & Fude Wang⁽⁴⁾ in which they had use Gaussian beam and we had used frustum beam for analysis of the beam on a model of length 36×4.8×6.00 mm on which the above part is there of dimensions 30×2.4×6.00 mm is there, in the above paper a case study is taken in to consideration in which top most two layer is been added by laser additive manufacturing which is been shown in the figure by brown colour, for this they had used commercially used ABAQUS and for doing so we had use ANSYS 14.0. For which the coding is given below.

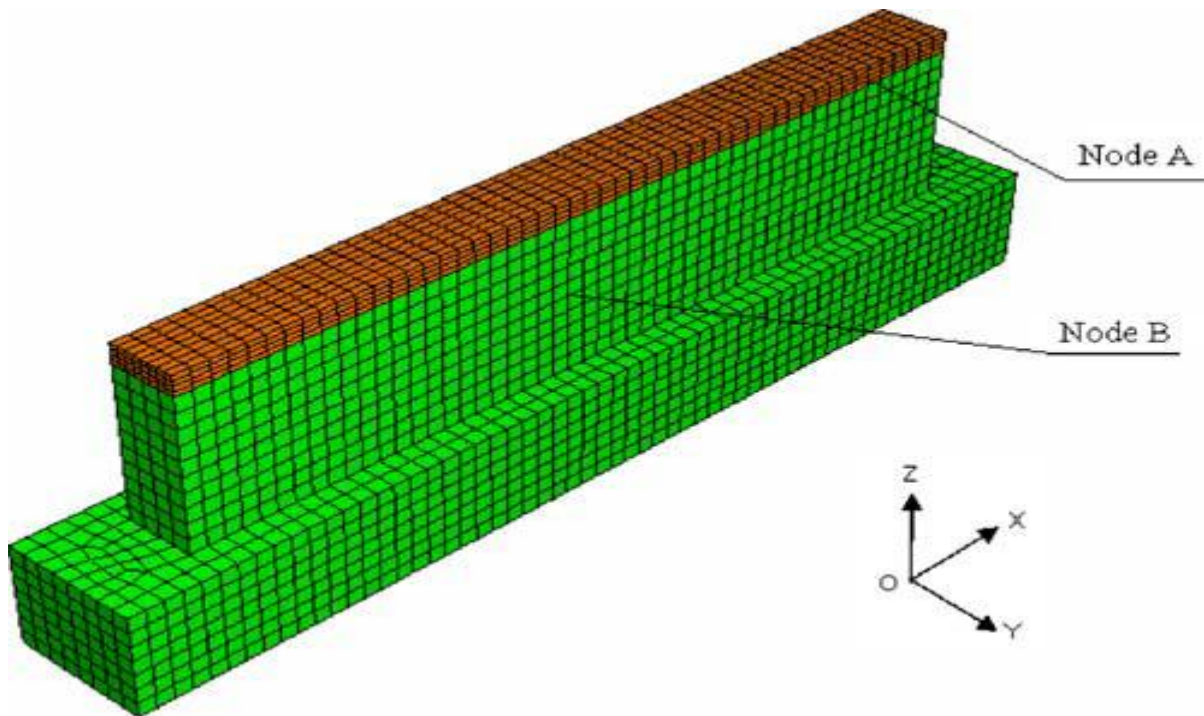


Figure 48 Model of work⁽³⁾

The coding for the ANSYS is:

finish

/clear,all

/prep7

et,1,278

n,0,0,0

ngen,25,1,1,,0.0002

ngen,181,25,1,25,,0.0002

ngen,31,4525,1,4525,,,0.0002

n,140276,0.003,0.005,0.0018

ngen,34,1,140276,,,0.0002

ngen,151,34,140276,140309,,0.0002

ngen,13,5285,140276,145409,,,0.0002

e,1,26,4551,4526,2,27,4552,4527

egen,24,1,-1

egen,180,25,-24

egen,30,4525,-4320

*do,j,0,11,1

*do,i,0,149,1

e,41125+25*i+4525*j,41150+25*i+4525*j,45675+25*i+4525*j,45650+25*i+4525*j,140276
+34*i+5285*j,140310+34*i+5285*j,145595+34*i+5285*j,145561+34*i+5285*j

*enddo

*enddo

.....

.....

.....

.....

.....

.....

.....

*do,i,0,11,1

time,0.5*(i+1)+42

nsel,s,node,,188044+408*i

```
nselect,a,node,,188078+408*i
nselect,a,node,,193295+408*i
nselect,a,node,,193397+408*i
nselect,a,node,,198580+408*i
nselect,a,node,,198682+408*i
nselect,a,node,,203899+408*i
nselect,a,node,,203933+408*i

f,all,heat,5

nselect,s,node,,193329+408*i
nselect,a,node,,193363+408*i
nselect,a,node,,198614+408*i
nselect,a,node,,198648+408*i

f,all,heat,15

nselect,all

solve

fdelete,all,heat

*enddo
```

Which give the below result with the nodal heat solution done in it.

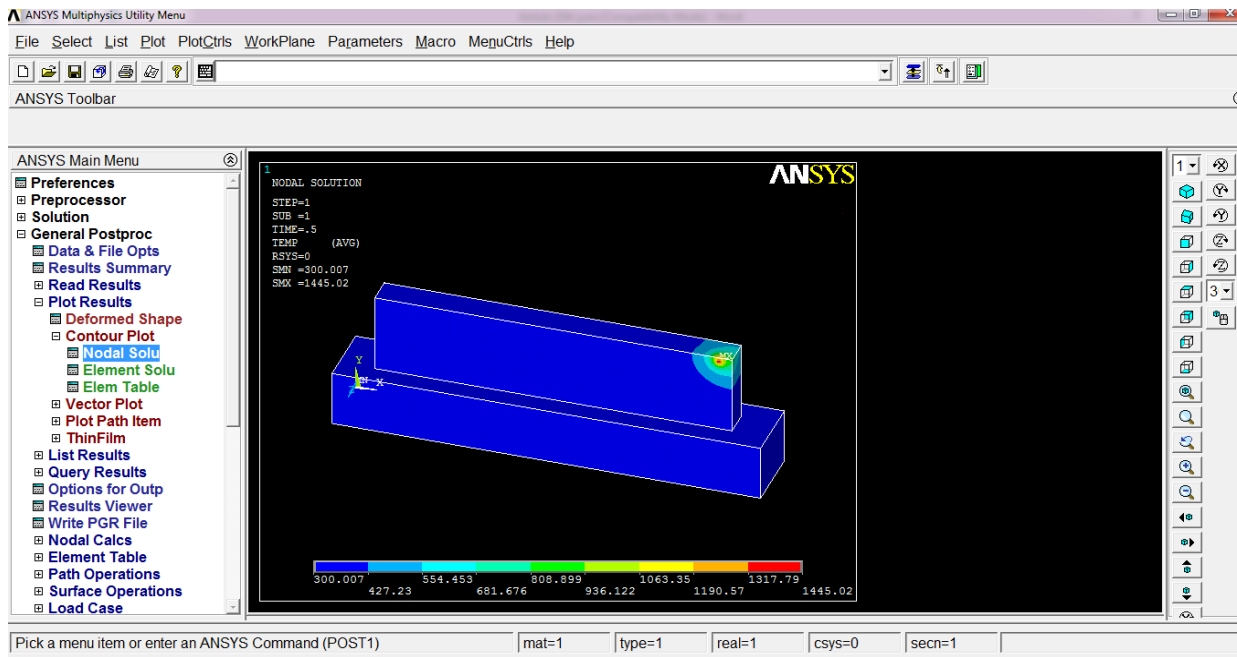


Figure 49 Nodal solution of temp.

The results is been discussed in result chapter

Chapter 4 Results

While taking the NODE A in the region where the beam start the additive manufacturing the graph come out to be similar but the value of peak temperature is found to be less as compared to the peak temperature found by et.al Jia Yang & Fude Wang⁽⁴⁾ by taking the laser values to be 800Watt power;300mm/min scanning speed; laser beam diameter to be 0.6mm;0.25 spectral absorptivity of nickel. The laser movement on the work piece is shown in figure.

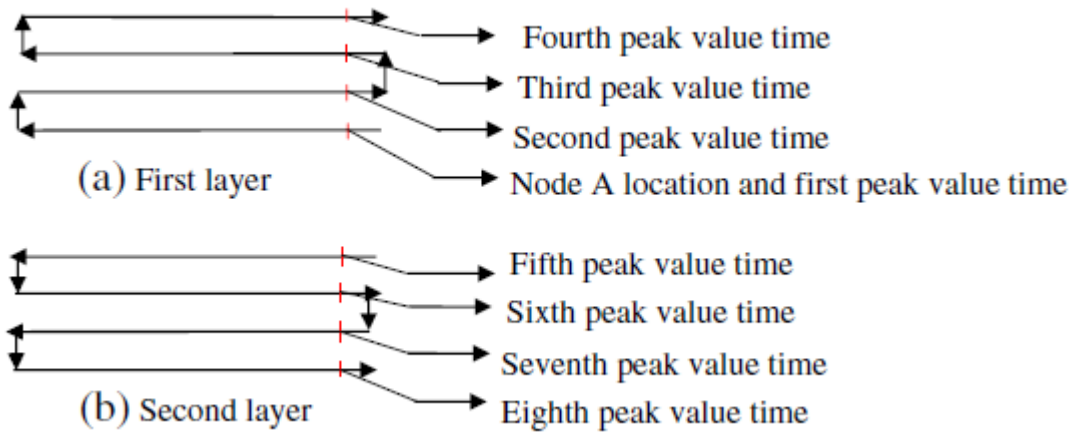


Figure 50 Peak value temperatures corresponding to time stages ⁽³⁾

By this way the peak temperature should be in order of below figure

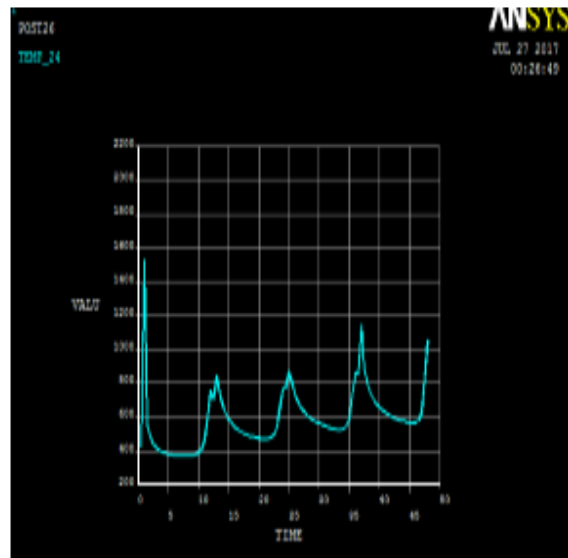
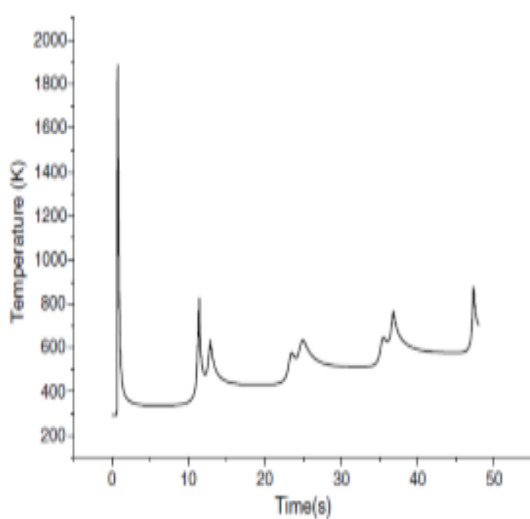


Figure 51 Compression between NODE A temp

The graphs of NODE B in et.al Jia Yang & Fude Wang⁽⁴⁾ and developed by our model are,

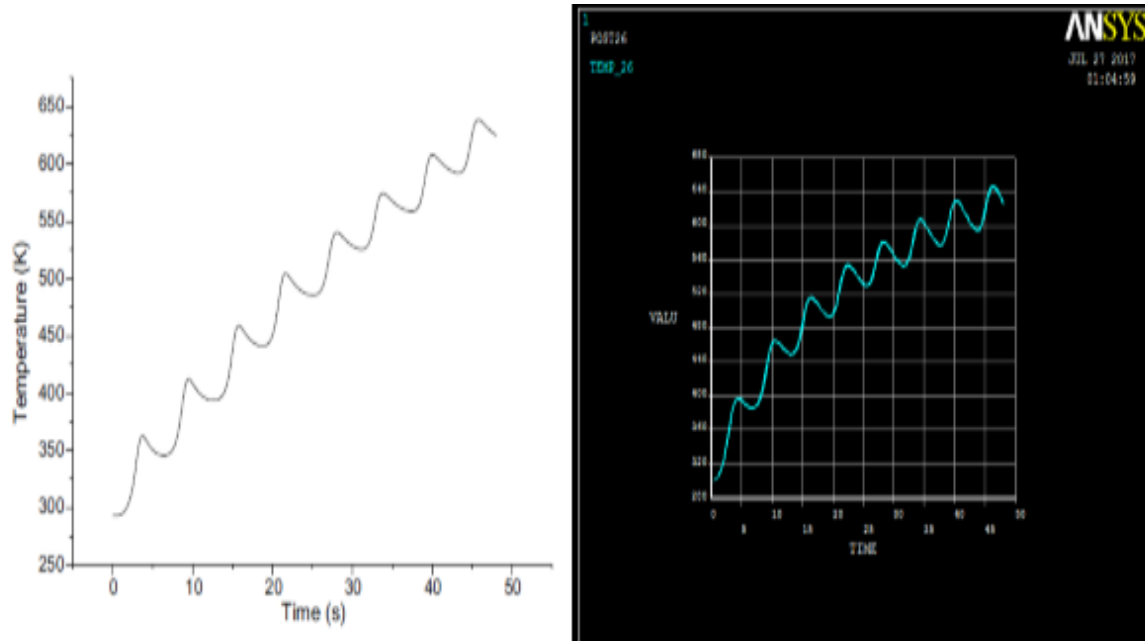


Figure 52 Compression between NODE B temp

Comparison

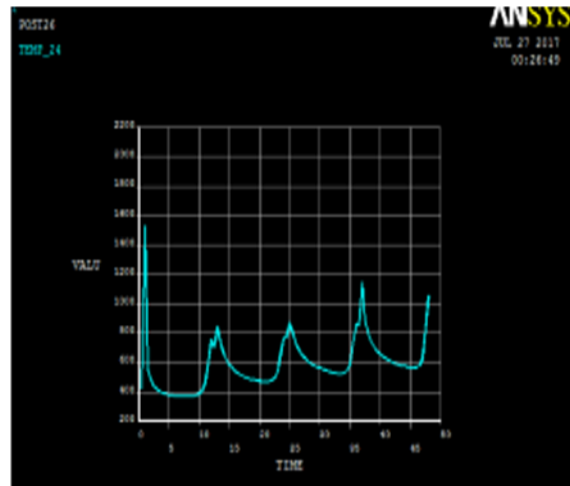
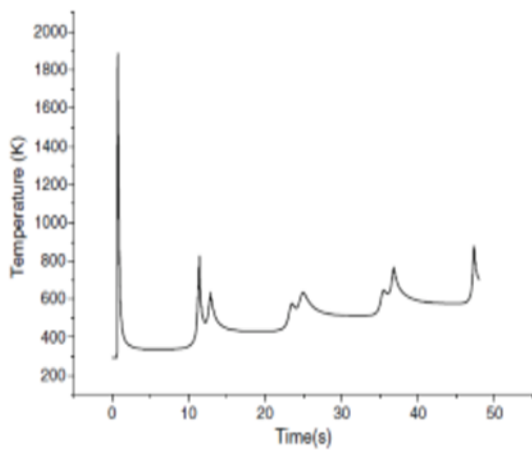
Time (sec)	Temperature in authors paper	Temperature given by our solution	Comparison
1	1888.22	1529.17	19%
5.5	336.77	375.39	13%
18.5	431.96	487.34	12%
28.5	521.95	592.75	13%
38	628.16	794.53	17%
46	612	578.44	10%

Chapter 5 Conclusion and future scope

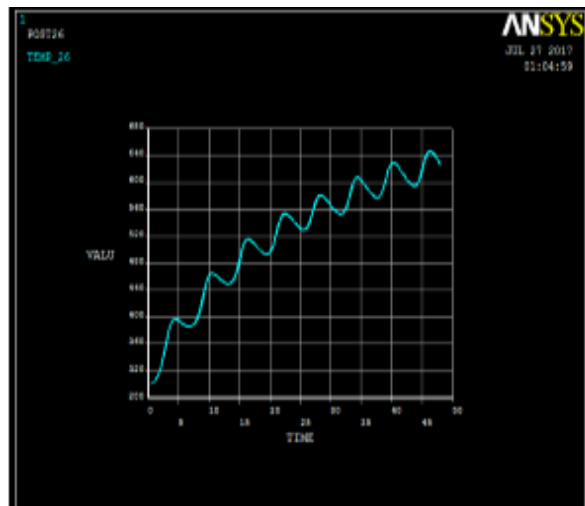
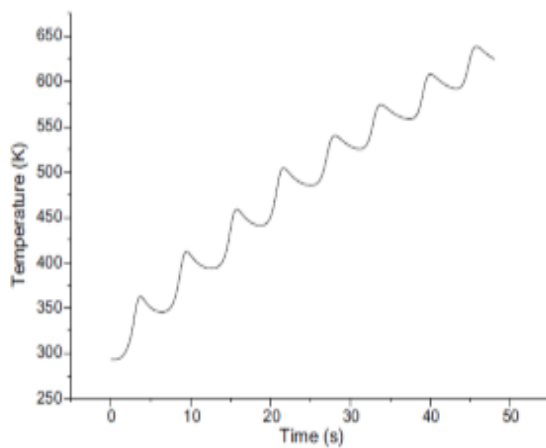
5.1 Conclusion

Comparison between two types of laser beam is done in this study, it is found that the type of laser beam can have a significant effect on peak temperature of the model which can lead to different type of micro structure of produce product on the basis of maximum temperature. The peak temp of Gaussian type of beam is found to be 1888K whereas the peak temperature of frustum beam is found to be 1529K (Approx.). Due to which many structural changes can be experienced while developing a new product. And the added layer can have different type of properties other than the whole material.

The peak temperature difference found out to be expressed by the following graphs.



And the temperature of the other NODE B is



5.2 Future Scope

By using LDMD (Laser Direct Metal Deposition) analysis in ANSYS the concept of element death and birth can easily explained which can ease the approach towards non similar metallic part testing in it. By using this most realistic beam can be explained and design and can be analysed for practical loads like temperature loads and structural loads. This can be done easily as meshing any complex structure is very easy in ANSYS, and fine and better meshing will lead to very accurate answers from the analysis. In thermal analysis each conduction, convection and radiation can be consider on a single subject, specially radiation can be solved very easily and efficiently, radiation on single surface of concepts of absorptivity, emissivity, reflectivity can be easily taken into consideration. Along with that many more time related parameter can be filled into this for better and exact results.

Reference:

- [1] <http://www.industrial-lasers.com/articles/print/volume-250/issue-6/features/laser-metal-deposition.html>
- [2] Song Jianli, Liu Zhiqi, QI Huiping, DU Shiwen, LI Yongtang, Deng Qilin (2008), Numerical simulation of the three-dimensional temperature field in Laser cladding forming process
- [3] V. Neela, A. De (2009) Three-dimensional heat transfer analysis of LENS process using finite element method, *International Journal on Advanced Manufacturing Technology* (2009) 45:935–943
- [4] Jia Yang, Fude Wang (2008) 3D finite element temperature field modelling for direct laser fabrication, *International Journal on Advanced Manufacturing Technology* (2008) 43:1060-1068
- [5] Yongjie Zhang, Gang Yu*, Xiuli He, Weijian Ning, Caiyun Zheng Numerical and experimental investigation of multilayer SS410 thin wall built by laser direct metal deposition
- [6] Wang, L., Felicelli, S., Gooroochurn, Y., Wang, P.T., Horstemeyer, M.F., (2008) optimisation of the LENS process for steady molten pool size. *Mater. Sci. Eng.* 148-156
- [7] Zhang YongJie, YU Gang & HE XiuLi, Numerical study of thermal history in laser aided direct metal deposition process, 2012
- [8] Atul Kumar, C.P. Paul, A. K. Pathak, P. Bhargava, L. M. Kukreja, (2012), A finer modeling approach for numerically predicting single track geometry in two dimensions during Laser Rapid Manufacturing, *Optics and Laser technology* 44,555-565
- [9] V.D. Manavatkar, A. A. Gokhale, G. Jagan Reddy, A. Venkataramana and A. De, (2011) Estimation of melt pool dimensions, thermal cycle, and hardness distribution in the Laser Engineered Net Shaping process of austenitic stainless steel, *The minerals, metals and materials society and ASM international*
- [10] Gangxian Zhu, Anfeng Zhang, Dichen Li, Yiping Tang, Zhiqiang Tong & Qiaopan Lu (2011) Numerical simulation of thermal behaviour during laser direct metal deposition *International Journal on Advanced Manufacturing Technology* 55:945-954
- [11] M. Labudovic, D. Hu, R. Kovacevic (2003) A 3D model for direct laser metal powder deposition and rapid prototyping. *Journal of Material science*, volume 38, issue 1, pp 35-49
- [12] P Peyre, P Aubry, R Fabbro, R Neveu, and A Longuet (2008) Analytical and numerical modelling of the direct metal deposition laser process, *Journal Physics D: Applied Physics* 41 (10pp)

- [13] Heng Liu, Todd E. Sparks, Frank W. Liou, David M. Dietrich,(2013), Numerical Analysis of thermal stress and deformation in Multi-Layer Laser Metal Deposition Process
- [14] V. Verma, and M. Shukla, Laser metal deposition thermal analysis using finite element method, *Proceedings of the 15th International RAPDASA conference*, Stellenbosch, South Africa, November 2014.
- [15] V. Verma, Finite Element Analysis of Laser Metal Deposition, *M.Tech. Thesis* (unpublished), Mechanical Engineering Department, MNNIT Allahabad, India, 2014.
- [16] M.Shukla, and V.Verma, Finite Element Simulation and Analysis of Laser Metal Deposition, 6th International Conference on Mechanical, Production and Automobile Engineering (ICMPAE'2014) Cape Town, South Africa, Nov. 27-28, 2014
- [17] <http://www.industrial-lasers.com/articles/print/volume-250/issue-6/features/laser-metal-deposition.html>
- [18] [https://en.wikipedia.org/wiki/Cladding_\(metalworking\)](https://en.wikipedia.org/wiki/Cladding_(metalworking))
- [19] <http://www.mece.ualberta.ca/tutorials/ansys/AT/Coupled/Coupled.html>